Nano Research

Open Access

Review Article

Revolutionizing breast cancer detection: Advances in fluorescent probe technology

Qian Gao[1], Lin Tang[2], Jun Zhan[3], Yiyuan Xue[1], and Feng Luo[1,4] ✉

[1] *State Key Laboratory of Oral Diseases & National Center for Stomatology & National Clinical Research Center for Oral Diseases, West China Hospital of Stomatology, Sichuan University, Chengdu 610041, China*
[2] *Emergency Obstetrics and Gynecology, West China Second University Hospital, Sichuan University, Chengdu 610041, China*
[3] *Department of Obstetrics and Gynecology, West China Second University Hospital, Sichuan University, Chengdu 610041, China*
[4] *Department of Prosthodontics, West China School of Stomatology, Sichuan University, Chengdu 610041, China*

Cite this article: *Nano Research*, **2025**, *18*, 94907079. https://doi.org/10.26599/NR.2025.94907079

ABSTRACT: With the increasing incidence of breast cancer globally, there is an urgent demand for enhanced diagnostic and therapeutic strategies. This comprehensive review explores advancements in fluorescent probe technology for breast cancer imaging and early diagnosis. Fluorescent probes offer unparalleled sensitivity and specificity in detecting cancer biomarkers, enabling early diagnosis and delineation of tumor margins during surgery. We categorize these probes into molecular, nano, ratiometric, the second near-infrared window (NIR-II), and multifunctional varieties, each with unique capabilities for targeting specific cancer markers. This review highlights recent innovations in probe design, emphasizing their applications in pathogenesis studies, drug development, precision medicine, and fluorescence-guided surgery. Despite their promising clinical potential, challenges such as safety, biomarker targeting accuracy, system compatibility, and clinical translation persist. Addressing these hurdles is crucial for the integration of fluorescent probes into standard cancer care, aiming to improve treatment outcomes and patient quality of life.

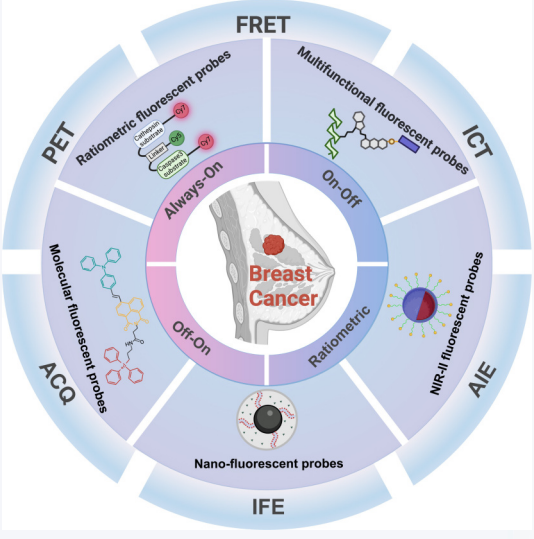

KEYWORDS: breast cancer, fluorescent probes, imaging, early diagnosis, biomarker

1 Introduction

Breast cancer remains one of the most prevalent cancers among women globally and is a substantial public health concern [1–3]. Its incidence has been on an upward trajectory for approximately four decades, highlighting the urgency for effective diagnostic and therapeutic strategies [4, 5]. In the treatment of nonmetastatic breast cancer, the primary objective is complete eradication of the tumor to prevent recurrence [6]. In contrast, for advanced stage IV breast cancer, which is characterized by distant metastases, recent research has indicated that removal of the primary tumor can improve patient prognosis [7]. Despite these approaches, the risk of recurrence persists for 10–32 years posttreatment, with approximately 30.1% of patients with breast-conserving surgery undergoing multiple surgeries [8, 9]. This is particularly notable in cases of triple-negative breast cancer (TNBC), where the rate of recurrence within five years postsurgery can be as high as 30%–40% in the operable setting [10].

Advancements in imaging technologies have been significant, yet the efficacy of tumor removal still heavily relies on the surgeon's expertise [11–13]. Traditional imaging modalities such as mammography, ultrasound, and magnetic resonance imaging (MRI) play critical roles in the detection of breast cancer [14–16]. Nonetheless, they often encounter limitations in sensitivity and specificity, especially during the early stages of the disease and in patients with dense breast tissues [15, 17–19]. Furthermore, intraoperative pathologic methods such as frozen section analysis are hindered by their complexity and time-intensive nature [20]. In the realm of artificial intelligence, there is still insufficient evidence to determine its accuracy and optimal use in breast cancer screening [21]. Consequently, identifying smaller lesions during

Received: July 3, 2024; **Revised:** September 13, 2024
Accepted: October 17, 2024

✉Address correspondence to luofeng0122@scu.edu.cn

surgery and diagnosing tumors early with conventional equipment are often challenging [11, 22].

In this context, the development of fluorescent probes for medical imaging represents a significant advance in oncological diagnostics. Fluorescent probes, specialized substances that exhibit fluorescence in the ultraviolet–visible–near infrared spectrum, have been increasingly utilized to detect and image breast cancer biomarkers [23]. They offer several advantages over traditional imaging methods, including higher sensitivity, cost-effectiveness, simplicity, rapid operation, and safety [24–26]. These probes enable real-time visualization of cellular and molecular processes, making them promising approaches for detecting early-stage tumors and aiding in fluorescence-guided surgery [14, 27].

Fluorescent probes can be categorized based on their fluorescence signal behavior into "always-on" and activatable types. The activatable fluorescent probes operate through diverse mechanisms such as intramolecular charge transfer (ICT) [28, 29], fluorescence resonance energy transfer (FRET) [30, 31], photoinduced electron transfer (PET) [32, 33], inner filter effect (IFE) [34–36], aggregation-caused quenching (ACQ) [37, 38], and aggregation-induced emission (AIE) [39–41]. A comprehensive understanding of these mechanisms is crucial for the development of novel fluorescent probes. Wang et al. [42] developed AuNCs@ZIF-8 and Zn_2Ph_2Da based ratiometric fluorescent probes with the FRET effect, and optimized fluorescence-labeled aptamers to increase the sensitivity of the probes. Gao et al. [43] discovered that the twisted conformations of rotor-rich compounds can enhance the fluorescence signal through the AIE effect and developed a TPA-TQ3 probe with both high fluorescence (FL) and photoacoustic (PA) signals for *in situ* breast tumor imaging. Additionally, these probes can be classified based on their size into molecular probes and nanoprobes [44]. They also encompass ratiometric probes that minimize background signal interference [45], NIR-II fluorescent probes that penetrate deeper into tissues (approximately 5–20 mm) [46], and multifunctional probes that combine different imaging modalities or integrate imaging with treatment, addressing multiple clinical needs simultaneously [47, 48].

This paper aims to thoroughly explore the principles, developments, and applications of fluorescent probes in breast cancer imaging and early diagnosis. We will examine how these probes specifically target cancer cells, their superiority over conventional imaging techniques, and the challenges they face. Furthermore, we will discuss recent progress in probe technology and the prospects of fluorescence imaging in breast cancer detection and management. By providing a comprehensive overview of fluorescent probes in the context of breast cancer, this paper highlights the transformative potential of this technology in reshaping cancer diagnosis and treatment landscapes (Fig. 1).

2 Principles of fluorescent probes

2.1 Modes of fluorescence response in probes

Fluorescent probes are primarily categorized based on their fluorescence signal dynamics into two modes: "always-on" and

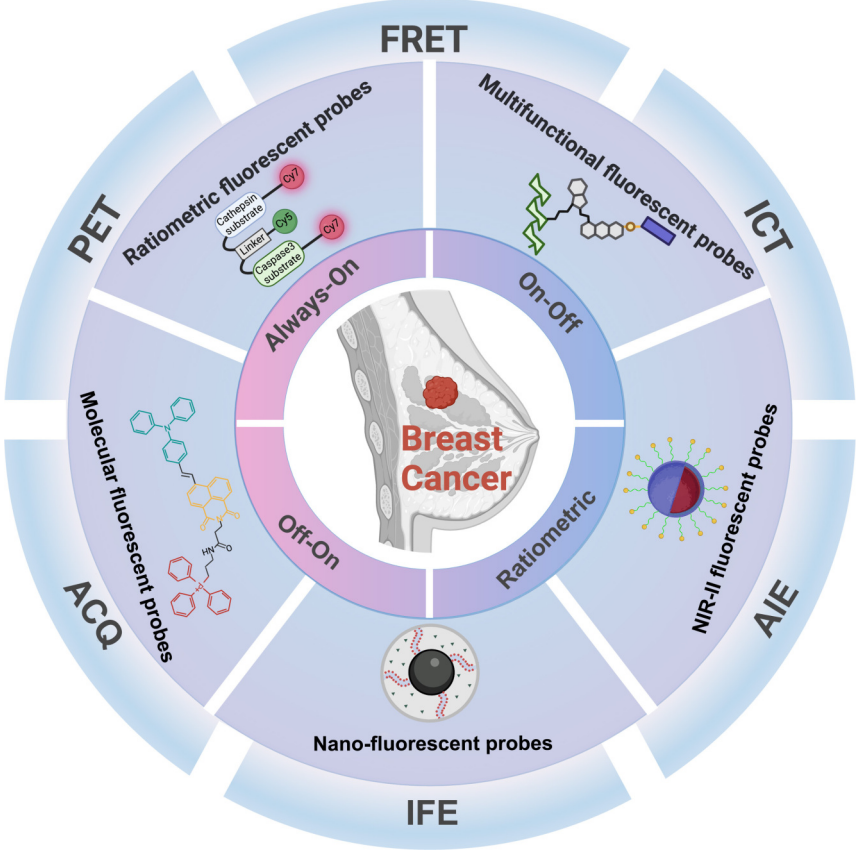

Figure 1 An overview of advances in fluorescent probes for breast cancer diagnosis and treatment. The inner layer shows the modes of fluorescence response in probes, the middle layer shows the categories of fluorescent probes targeting breast cancer, and the outer layer shows the mechanisms of fluorescence response in activatable probes. The figure was created with BioRender.com.

activatable. The "always-on" mode functions through constant fluorescence emission, which is utilized primarily for imaging via accumulation at specific sites. Conversely, the activatable mode interacts dynamically with target molecules, altering either the fluorescence wavelength or intensity. This activatable mode can be further subdivided into three types: "off-on", "on-off", and ratiometric, each characterized by distinct fluorescence response patterns in the presence of the target molecule (Fig. 2(a)) [49–52].

2.2 Mechanisms of the fluorescence response in activatable probes

Activatable fluorescent probes generally comprise three components: a fluorophore, a linker, and a recognition group [53]. The interaction between the recognition group and the target molecule induces a change in the fluorescence signal [54]. This interaction can be explained through several response mechanisms, including ICT, FRET, PET, IFE, AIE, and ACQ. A brief overview of these mechanisms is provided below.

2.2.1 *ICT mechanism*

ICT-based fluorescent probes consist of a fluorophore, an electron donor, and an electron acceptor, creating a "push-pull" molecular system. Interaction with the target molecule alters the electron pushing or pulling capabilities, leading to shifts in the fluorescence spectrum, either blue or red (Fig. 2(b)) [28, 29].

2.2.2 *FRET mechanism*

FRET involves non-radiative energy transfer between donor and acceptor molecules. Upon light excitation, the excited donor transfers energy to the ground-state acceptor, necessitating spectral overlap between the donor's emission and the acceptor's absorption spectra [30]. In the absence of a target molecule, the donor's fluorescence is quenched because of energy transfer to the acceptor. However, the presence of a target molecule disrupts this interaction, restoring the donor's fluorescence (Fig. 2(c)) [31].

2.2.3 *PET mechanism*

PET-induced fluorescence quenching occurs when the electron energy levels of the acceptor lie between the highest occupied and lowest unoccupied molecular orbital (HOMO and LUMO) of fluorophore. Binding to a target molecule alters the receptor's HOMO energy, interrupting the PET process and reinstating fluorescence (Fig. 2(d)) [32, 33].

2.2.4 *IFE mechanism*

IFE involves the absorption of a fluorophore's excitation or emission by another absorbing substance. It requires spectral overlap between the fluorophore and absorber, differing from FRET in that it involves radiative energy transfer and offers more flexibility in the distance between interacting molecules (Fig. 2(e)) [34–36].

2.2.5 *ACQ mechanism*

ACQ describes the reduction or disappearance of fluorescence intensity when a fluorophore is in a high concentration or solid state, often due to self-quenching or interactions with quenchers influenced by hydrogen bonding or electrostatic attraction (Fig. 2(f)) [37, 38].

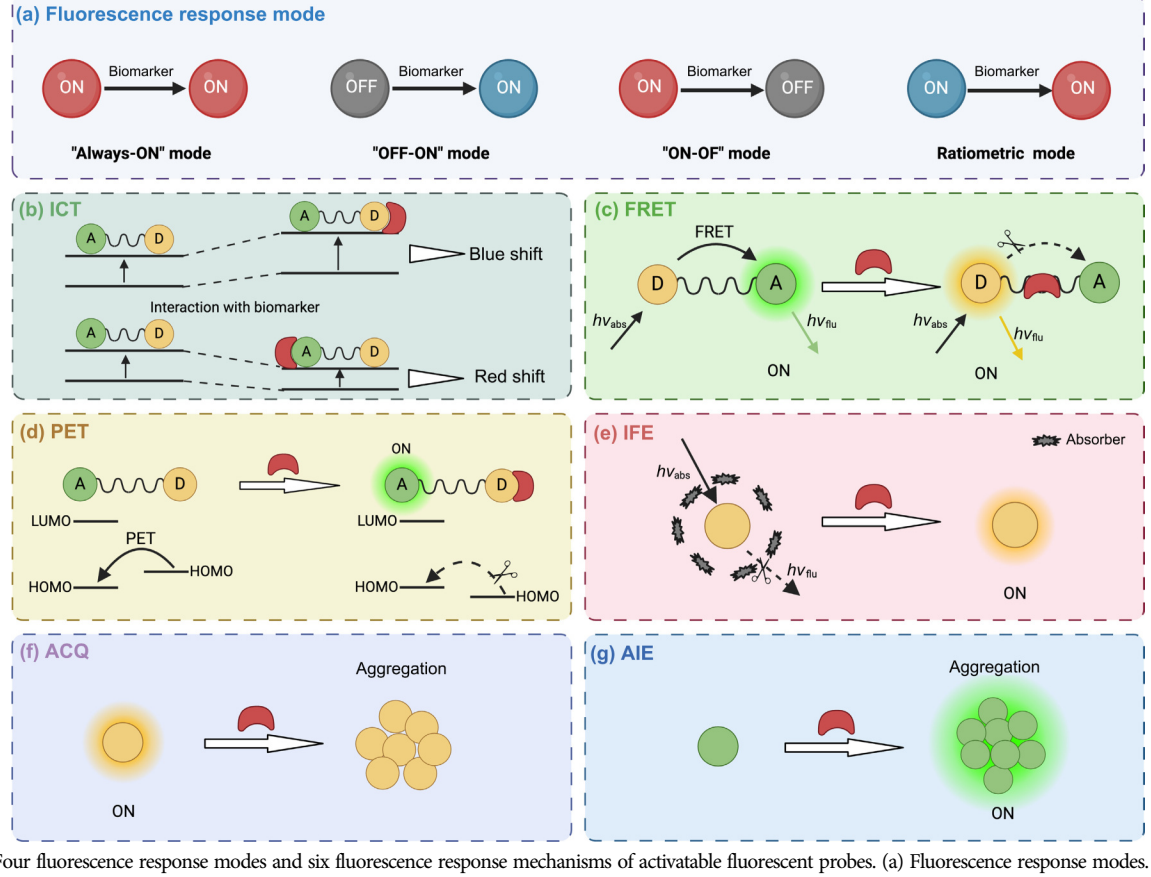

Figure 2 Four fluorescence response modes and six fluorescence response mechanisms of activatable fluorescent probes. (a) Fluorescence response modes. (b) ICT. (c) FRET. (d) PET. (e) IFE. (f) ACQ. (g) AIE. A, acceptor; D, donor. The figures were created with BioRender.com.

2.2.6 *AIE mechanism*

In contrast to ACQ, AIE denotes a significant increase in fluorescence intensity when fluorophores aggregate or are in the solid state, which is typically weakened or non-emissive in dilute solutions. This is attributed to restricted intramolecular rotation and vibration in the aggregated state, blocking non-radiative decay pathways and resulting in amplified emission (Fig. 2(g)) [39–41].

3 The diverse categories of fluorescent probes for breast cancer imaging and early diagnosis

Since their inception, fluorescent probes have garnered significant interest, evolving from molecular to nano-fluorescent probes, with ongoing advancements in probe development and modification. A pivotal moment occurred in 2009 when Hongjie Dai and colleagues discovered that single-walled carbon nanotubes could emit NIR-II fluorescence [55]. This NIR-II range (1000–1700 nm) offers reduced light scattering in biological tissues compared with the first near-infrared window (NIR-I, 700–900 nm), thereby enhancing *in vivo* imaging capabilities [56, 57]. This breakthrough has substantially accelerated the development of NIR-II fluorescent probes. Similarly, modified ratiometric probes have demonstrated enhanced properties, significantly mitigating background signal interference and improving the accuracy of fluorescent probes for breast cancer detection and monitoring [58]. Currently, fluorescent probes have become indispensable tools in the medical field through the detection of specific biomolecules involved in disease occurrence and progression (including ions, reactive species, and enzymes), many of which are promising for the treatment of breast cancer [59]. In recent years, with the in-depth study of breast cancer, an increasing number of biomarkers have been discovered, which also provides an opportunity for the development of fluorescent probes for breast cancer imaging and early diagnosis.

3.1 Molecular fluorescent probes

In the realm of fluorescence imaging, there has been a pronounced reliance on small molecule-based dyes, notably coumarin and fluorescein, which are favored for their exceptional biocompatibility and flexibility afforded by chemical modification [60]. These small-molecule fluorescent probes are specifically engineered to target distinct cellular components, including organelles, enzymes, and unique microenvironments within biological systems [61]. The burgeoning interest in organelle-targeting probes is particularly notable, offering promising avenues for the development of novel disease treatment strategies [62]. These probes are characterized by their ability to facilitate nondestructive and rapid analysis, customizable structural design, cost-effectiveness and high sensitivity and are increasingly recognized as potent tools for the detection of breast cancer [63].

Emerging research has revealed a notable difference in the average polarity between cancer cells and their normal counterparts, emphasizing that cancer progression is accompanied by diverse changes in organelles [64]. A critical focus has been on mitochondrial signal transduction, a key player in essential cellular processes such as aerobic respiration, cell proliferation, and apoptosis. The imbalance of reactive oxygen species (ROS), often associated with the progression of cancer, further necessitates a detailed investigation of mitochondrial polarity in the context of breast cancer pathology [65].

In this vein, Yin et al. [66] developed a novel fluorescent probe, termed PNN, designed to investigate changes in mitochondrial polarity associated with breast cancer. This study revealed a decrease in mitochondrial polarity during the carcinogenesis of breast cancer epithelial tissue. PNN, which functions through the ICT effect, exemplifies a "push-pull" molecule comprising a targeted group (triphenylphosphine cation), a receptor (1,8-naphthalimide), and a donor (triphenylamine group). The specificity of PNN for mitochondria stems from the affinity of triphenylphosphine cations for the mitochondrial membrane potential. Upon excitation, PNN undergoes electron transfer from the ground state to a locally excited state, with the fluorescence intensity being contingent upon mitochondrial polarity. High mitochondrial polarity leads to a strong solvation relaxation process between PNN and the solvent, predominantly resulting in non-radiative energy dissipation and thus weaker fluorescence. In contrast, lower mitochondrial polarity results in the predominance of radiative energy release, manifesting as stronger fluorescence (Fig. 3(a)). This study not only highlights mitochondrial polarity as a potential biomarker for breast cancer detection but also paves the way for innovative approaches in mitochondrial polarity imaging.

Moreover, cytochrome P450 1A1 (CYP1A1), an extrahepatic enzyme implicated in converting procarcinogens into DNA-damaging agents, has been reported to be constitutively expressed in breast cancer cells [67]. Liu et al. [68] introduced a novel approach for tracking the metastasis and invasion pathways of breast cancer cells using CYP1A1-activated fluorescent probes. The selected probe DCBEM incorporates a dicyanoisophorone derivative as the fluorophore, coupled with a CYP1A1 recognition group (O-chloroethyl) and a leaving group. The O-chloroethyl component serves a dual function, acting as an enzymatic reaction site for CYP1A1 and quenching the fluorescence of the fluorophore by shielding the electron donor. In the presence of CYP1A1, the recognition group undergoes hydrolysis, converting the ether bond to a hydroxyl group and restoring the ICT effect, thereby activating the fluorescence signal. This cascade reaction leads to the removal of the leaving group, forming the CYP1A1-DCBEAM conjugate (Fig. 3(b)). The localization of CYP1A1 in the endoplasmic reticulum enables this fluorescent probe to be employed for long-term tracking of breast cancer cells, successfully delineating the metastasis pathway of MCF-7 cells in mice, including the route "intestine → liver → lung → kidney" (Fig. 3(c)).

In general, compared with conventional probes that begin to diffuse freely once they enter the cell matrix, the abovementioned small-molecule fluorescent probes that can target specific organelles should be more applicable in practical studies. However, autofluorescence from endogenously abundant cellular molecules can cause significant interference with imaging, which can be improved by selecting optimal excitation and emission wavelengths. In addition, many organelles, such as microtubules and lipid droplets, await further study [69]. We believe that fluorescent probes targeting organelles will be powerful tools for understanding cellular processes.

3.2 Nano-fluorescent probes

Recent advancements in nanomaterial research have significantly impacted various medical fields, including targeted drug delivery, imaging, and diagnosis [70]. Nanoparticles, characterized by their excellent biocompatibility, high stability, and superior loading rates, are particularly notable. Their inherent fluorescence, ease of modification and other physicochemical properties make them ideal for customization. The functionalization of nanoparticle

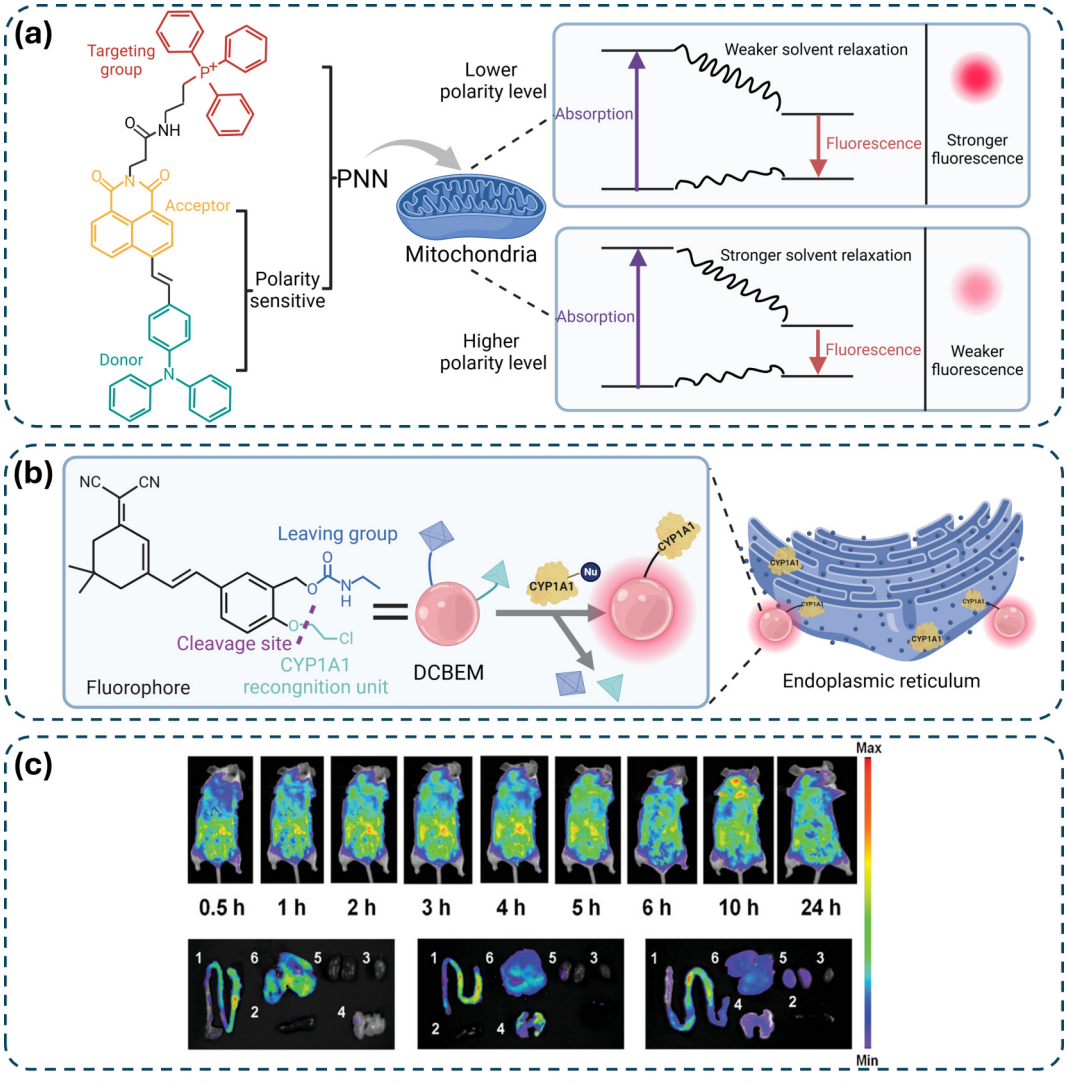

Figure 3 Imaging process of molecular fluorescent probes and fluorescence images of DCBEM tracking of MCF-7 cells *in vivo*. (a) The structure of PNN and its mechanism for detecting mitochondrial polarity in breast cancer. (b) The structure of DCBEM and the process of targeting CYP1A1. (c) *In vivo* imaging of live mice at different times and fluorescence images of vital organs (1: intestine; 2: spleen; 3: heart; 4: lung; 5: kidney; 6: liver) at 4, 10, and 24 h after IV injection of DCBEM-labeled MCF-7 cells. (c) Reproduced with permission from Ref. [68], © Wiley-VCH GmbH 2023. The figures were created with BioRender.com.

surfaces with antibodies or small molecules enhances their targeting capabilities and efficacy in fluorescence imaging and early diagnosis [71–73]. Compared with small-molecule probes, nanoprobes offer enhanced stability, making them increasingly valuable in medical diagnostics, particularly in the detection of breast cancer [74]. Commonly used materials for creating nano-fluorescent probes include metal-organic frameworks (MOFs), gold nanoparticles (AuNPs), and quantum dots (QDs) [75, 76]. These materials serve dual purposes, acting both as carriers and fluorophores, thereby broadening the scope of their application in medical science.

3.2.1 *MicroRNAs (miRNA) targeting in breast cancer diagnosis*

MicroRNAs play pivotal roles in regulating the proliferation, invasion, and metastasis of breast cancer, and their expression levels are correlated with the stage of cancer [77, 78]. Notably, miRNAs, often encapsulated in vesicles as exosomal miRNAs, contribute to intercellular communication and maintain miRNA stability [79]. This has led to the recognition of miRNAs as potential biomarkers in breast cancer diagnostics. Zhao et al. [80] developed thermophoretic nanoflares for the *in situ* detection of exosomal miR-375 secreted by MCF-7 cells. This probe utilized spherical AuNPs prehybridized with Cy5-labeled complementary single-stranded DNA, whose fluorescence was quenched upon close association with Cy5. After incubation at 37 °C for 2 h, 22.5% of exosomal miRNAs was encapsulated with nanoflares, and the subsequent displacement of the Cy5-labeled DNA by miR-375 resulted in increased fluorescence (Fig. 4(a)). This novel approach demonstrated 85% accuracy in detecting early-stage (stage I, II) estrogen receptor (ER)-positive breast cancer.

Chen et al. [81] further advanced this field by constructing nanoprobes based on two-dimensional (2D) MOFs for dual miRNA detection in individual cancer cells. These nanoprobes successfully differentiated 10 mixed MCF-7 cells from 10^5 negative epithelial cells. The 2D Cu-TCPP MOF nanosheets were modified with polyethylene glycol (PEG)-conjugated polypeptides and then functionalized with miR-21 recognition sequences labeled with green dye (fluorescein amidite) and miR-10a sequences labeled with red dye (Texas-red), forming probes@MOF-PEG-peps. The fluorescence of these probes, quenched by the MOF nanosheets via the FRET effect, was restored when the probes entered a cell and

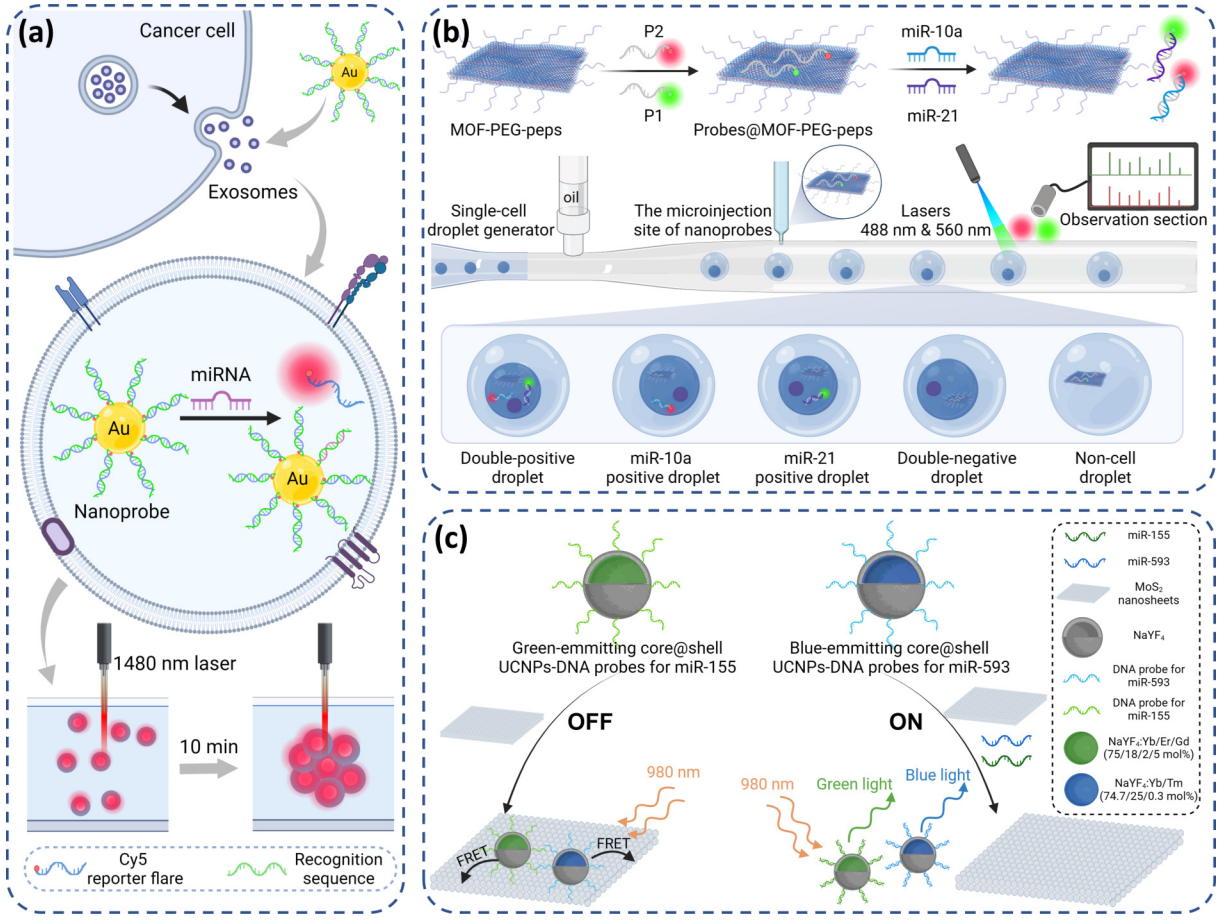

Figure 4 Mechanisms of nano-fluorescent probes in breast cancer diagnosis based on miRNA targeting. (a) Schematic of the mechanism by which nanoprobes detect the exosomal miRNAs, and the fluorescence signal is amplified by local 1084 nm laser heating. (b) A platform based on Probes@MOF-PEG-peps, with the droplet generator, the microinjection site, and the observation section, realizing the simultaneous detection of miR-21 and miR-10a in an individual cell. P1: fluorescein amidite-labeled miR-21 capture probe, P2: Texas-red-labeled miR-10a capture probe. (c) The scheme for detecting miRNAs with CSUDPs/MoS_2. The figures were created with BioRender.com.

hybridized with the target miRNA, detaching the double-stranded DNA from the MOF surface. For enhanced accuracy, these nanoprobes were integrated into a nanosensor, incorporating a microinjection site, a single-cell droplet generator, and an observation section (Fig. 4(b)). Upconversion nanoparticles (UCNPs), recognized for their ability to convert lower-energy NIR light into higher-energy ultraviolet or visible light, have also been utilized in this context [82, 83]. Wu et al. [84] developed a method integrating core@shell UCNP-DNA probes with MoS_2 nanosheets (CSUDPs/MoS_2) for miR-593 and miR-155 detection in breast cancer cells. CSUDPs/MoS_2, distinguished by varying molar ratios of lanthanide ions and attached ssDNA sequences, produced light emission under 980 nm laser irradiation. The fluorescence of these probes were quenched by MoS_2 nanosheets through the FRET effect, which was reversed upon hybridization with the target miRNAs (Fig. 4(c)). This sensor exhibited impressive sensitivity, with detection limits for miR-593 and miR-155 of approximately 0.17 and 0.25 nM, respectively.

3.2.2 *Receptor targeting in nanoprobe imaging*

QDs, semiconductor particles measuring 2–10 nm in diameter, have recently emerged as novel materials for imaging applications [85]. In a significant development, Kwon et al. [86] engineered a nanoprobe, anti-human epidermal growth factor receptor 2 (HER2)-PEG-QD, which demonstrated its efficacy in imaging MCF-7 cells and mouse models of breast cancer. Notably, the limit of detection (LOD) of the probe was as low as 500 μm from the skin. These FeSe QDs were synthesized via a one-pot process and are surface-coated with PEG to facilitate binding to HER2 antibodies (Fig. 5(a)). This binding enables the targeted imaging of HER2 receptors on MCF-7 cells. The QDs exhibit dual-photon excitation at 800 nm and triple-photon excitation at 1080 nm, with cyan light emission detectable at approximately 440 nm. This photoluminescence quality significantly enhances spatial resolution and penetration depth, making it invaluable for *in situ* cancer tissue imaging.

Further advancements in receptor targeting have been made by Guo et al. [87], who developed a glycoprotein nonmetastatic gene B (GPNMB)-targeting nanoprobe using QD520, with an emission maximum at 520 nm, and a HER2-targeting nanoprobe using QD620, with an emission maximum at 620 nm. This was specifically aimed at detecting TNBC. The nanoprobes were synthesized with QDs as the core and peptides modified by fatty acid chains as characteristic sequences for target proteins. The process involved a reverse microemulsion technique, where the hydrophobicity of the fatty acid chains caused the imprinted epitopes to protrude in the aqueous phase. The silylating reagents subsequently facilitated the imprinting process, filling the water

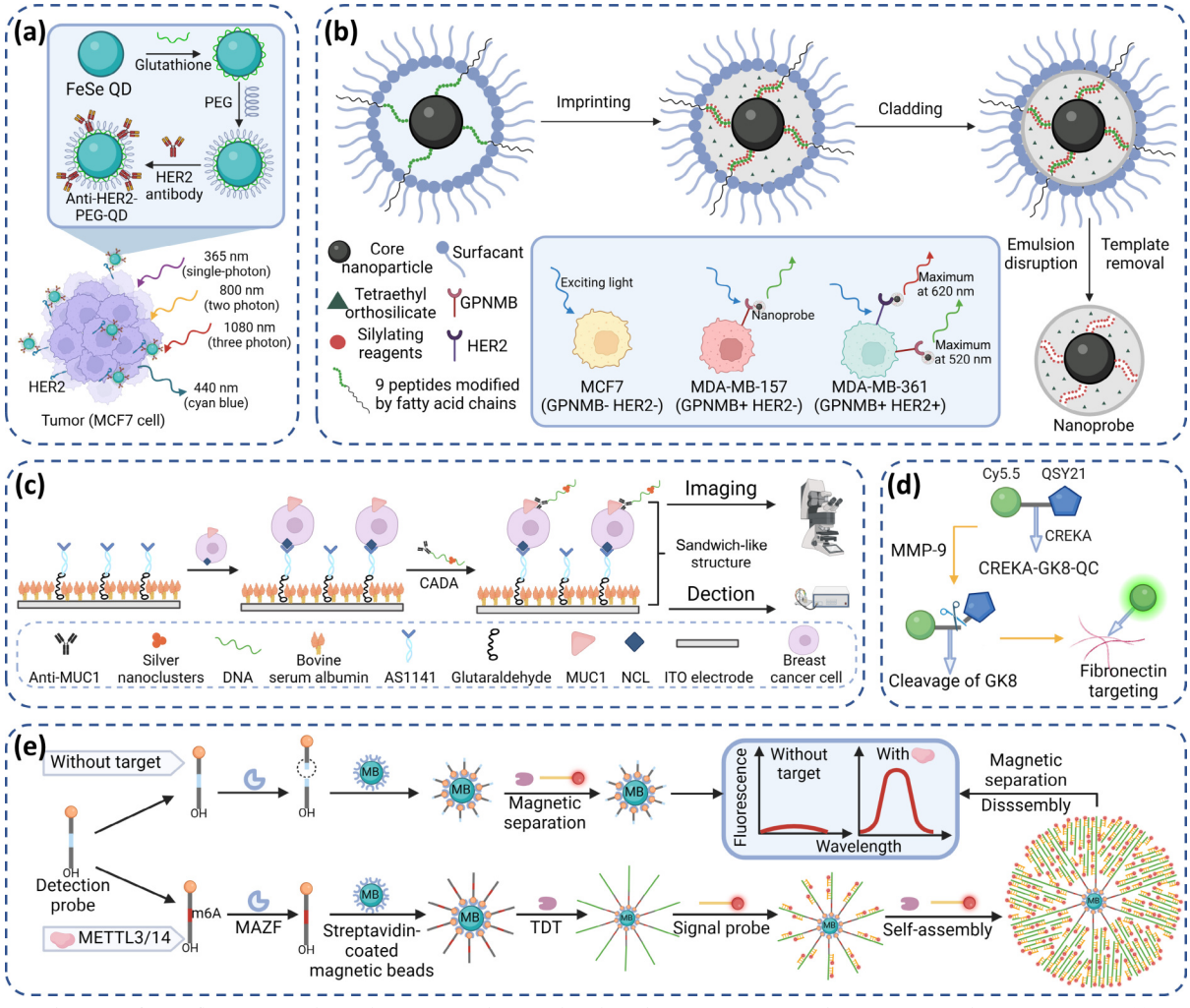

Figure 5 Mechanisms of nano-fluorescent probes in breast cancer diagnosis based on the receptor, transmembrane protein, and enzyme targeting. (a) Conjugation procedure for preparing Anti-HER2-PEG-QDs and their two-photon and three-photon excitation properties. (b) Schematic of the synthesis process and imaging principle of HER2 and GPNMB targeting nanoprobes. (c) An integrated system based on DNA template silver nanoprobes for imaging and detection of breast cancer cells. (d) Schematic illustration of fibronectin-targeting and MMP-9-activatable nanoprobes for breast cancer imaging. (e) A controlled amplification mechanism based on the detection probe and signal probe was used to detect METTL3/14, and the fluorescence signal was significantly different between the presence and absence of METTL3/14. The figures were created with BioRender.com.

phase with tetraethyl orthosilicate, which formed a silica layer to coat the nanospheres. The final step involved washing them to extract the templates, resulting in QD-cored cladded molecularly imprinted polymers (QD@cMIPs). The effectiveness of this method was validated in the human TNBC cells lines MDA-MB-157 (GPNMB+, HER2-), MDA-MB-361 (GPNMB+, HER2+), and MCF-7 (GPNMB-, HER2-) (Fig. 5(b)). Furthermore, *in vivo* experiments with male nude mice bearing MDA-MB-157 tumors demonstrated the effectiveness of the probe, particularly after the core QD520 of QD@cMIP was replaced with NIR797.

In addition to HER2 and GPNMB receptors, 70% of breast cancer patients are positive for hormone receptors, namely, the ER and progesterone receptor (PR) [88]. However, in recent years, few studies have focused on fluorescent probes that target hormone receptors, most of which are molecular fluorescent probes. For example, Tang et al. [89] developed the first ERα-targeted turn-off fluorescent probe, 2-((5'-(4-hydroxyphenyl)-2,2'-bithiazol-5-yl)methylene)malononitrile, for N_2H_4 imaging in breast cancer based on the ICT mechanism. Moreover, Barman et al. [90] designed an ER-targeting benzothiazole-purine hybrid molecular probe, CPIB, and induced the apoptotic death of the same cancer cells by targeting intracellular microtubules. The probe only analyzed tumor inhibition effect in three-dimensional (3D) tumor models of cancer cells, and the "detection and destroy" effect *in vivo* needs further study. Zhang et al. [91] designed genetically engineered responsive elements consisting of specific DNA fragments and auxiliary sequences. By reacting with ER/PR proteins and enhancing their downstream target gene (near-infrared fluorescent protein gene) expression, the probe achieved breast cancer imaging. Despite the successful detection of visible light emitted by ER/PR-positive cells under a near-infrared laser, the molecular probe failed to irradiate ER/PR tumors at the whole-body level.

3.2.3 *Targeting transmembrane proteins in breast cancer*

Mucin-1 (MUC1), a glycoprotein that is overexpressed in up to 90% of breast cancers, is linked to properties such as metastasis [92, 93]. Nucleolin (NCL), another significant biomarker, is found in abundance on the surface of breast cancer cells [94]. Capitalizing on these biomarkers, Cao et al. [95] developed an innovative system

incorporating DNA-templated silver nanoclusters (DNA-AgNCs) for simultaneous imaging and detection of breast cancer cells. The synthesis of these silver nanoclusters involved silver nitrate ($AgNO_3$), ammonium acetate (NH_4Ac), sodium borohydride ($NaBH_4$), and G-rich sequences. These clusters were then linked to Anti-MUC1 antibody via the Sulfo-SMCC crosslinker, creating (anti-MUC1 antibody)-(DNA-AgNCs) conjugates (CADA). The CADA nanoprobe, combined with a microscopy, forms the imaging component, while detection component involves an AS1141 aptamer-modified indium tin oxide (ITO) electrode and a signal detection device. When MCF-7 cells are introduced into the system, they bind to the ITO electrode via the interaction of NCL with the AS1141 aptamer. Simultaneously, these cells attach to the nanoprobe through MUC1, forming a sandwich-like structure.

This dual-recognition process (Fig. 5(c)) not only enhances the fluorescence signal but also amplifies the electrochemical signal, thereby significantly improving the detection accuracy. The LOD of this system has been determined to be as few as three cells, demonstrating its high sensitivity and potential for early breast cancer detection.

3.2.4 *Targeting enzymes in breast cancer diagnosis*

Matrix metalloproteinases (MMPs), known for their role in the NF-kB pathway, are instrumental in the progression of breast cancer invasion and metastasis [96]. In a significant advancement, Cheng et al. [97] developed a sophisticated fibronectin-targeting and MMP-9-activatable nanoprobe for fluorescence imaging of breast cancer. This probe, termed CREKA-GK8-QC, integrates a fibronectin-targeting peptide (CREKA), a near-infrared dye (Cy5.5), and a quenching agent (QSY 21), which are interconnected via an MMP-9-sensitive peptide sequence (GK8) (Fig. 5(d)). Upon administration in murine models, CREKA-GK8-QC effectively targets fibronectin, which is abundantly expressed in the TNBC microenvironment. The subsequent MMP-9-mediated cleavage of the GK8 sequence results in the activation of Cy5.5 fluorescence, enabling the precise localization and imaging of breast cancer lesions and their metastases to the lungs, which are nearly 1 mm in size.

In parallel, N6-methyladenosine (m6A) has been identified as a pivotal modifier in breast cancer RNA, influencing critical aspects such as RNA termination codons, the 5′ cap structure, and the 3′ untranslated region. The methylation process, a key aspect of m6A modification, is catalyzed by methyltransferases, which are linked to cancer cell migration and invasion [98]. Zhao et al. [99] innovatively employed detection and signal probes in a novel amplification mechanism to identify the (methyltransferase-like 3)-(methyltransferase-like 14) complex (METTL3/14). The detection probe, a biotin-modified DNA/RNA chimera, includes a specific RNA sequence, 5'-G-G-A-C-A-3', targetable by METTL3/14. This detection system operates in four critical phases: (1) methylation of the detection probe by METTL3/14 (methylation sequence 5'-G-G-m6A-C-A-3'), which hinders its cleavage by the ribonuclease MazF; (2) attachment of the probe to magnetic nanoparticles through biotin-streptavidin binding, facilitating the removal of unbound probes; (3) synthesis of a polyT sequence from the detection probe with the 3'-OH terminal as the primer, catalyzed by terminal deoxynucleotidyl transferase (TdT) in a template-independent DNA polymerization process; and (4) hybridization of this polyT sequence with a polyA-tailed, Cy5-labeled signal probe, forming a complex dendritic DNA nanostructure. In the final step, high-temperature disruption of the biotin-streptavidin bond enables the detection of Cy5 fluorescence. In the absence of METTL3/14, the detection probe is cleaved by MazF, preventing polymerization and thus not generating a fluorescence signal (Fig. 5(e)). This method boasts an LOD of 2.61×10^{-15} M and is capable of identifying METTL3/14 at the single-cell level.

3.2.5 *Additional nanoprobe varieties*

Semiconductor-conjugated polymer dots (PDs), which are primarily composed of π-conjugated polymers, measuring less than 40 nm in diameter, exhibit notable properties, such as intense fluorescence, robust stability, and the capacity for facile surface modification [100, 101]. Cytochrome C, whose release is recognized as a definitive biomarker due to its association with irreversible mitochondrial apoptosis, has been a focal point in nanoprobe development [102]. In this context, Shamsipur et al. [103] engineered a nanoprobe based on the ACQ effect for simultaneous imaging of Fe^{3+} and cytochrome C. This fluorescent nanoprobe, TBP@PFBT PDs, is synthesized by doping tributyl phosphate in the semiconducting polymer poly[(9,9-dioctylfluorenyl-2,7-diyl)-alt-co-(1,4-benzo-(2,1',3)-thiadiazole)]. The hydrophobic butyl group of tributyl phosphate integrates into the polymer matrix, whereas the hydrophilic phosphate group remains exposed on the surface of PDs. This design facilitates the chelation of Fe^{3+} and cytochrome C with phosphate groups, leading to the fluorescence quenching of TBP@PFBT PDs.

The efficacy of these nanoprobes was validated using doxorubicin, an inducer of apoptosis. In the absence of doxorubicin, cells treated with tributyl phosphate@polymer poly[9,9-dioctylfluorenyl-2,7-diyl)-co-1,4-benzo-{2,10-3}-thiadiazole)] (TBP@PFBT) PDs exhibited strong green fluorescence. However, upon doxorubicin treatment, a gradual decline in fluorescence intensity was observed, which coincided with the progression of apoptosis. This reduction, stabilizing during 24–48 h, is attributed to the apoptosis-induced release of cytochrome C and iron ions into the cytoplasmic matrix, which in turn quenches the fluorescence of the TBP@PFBT PDs. These findings underscore the potential of TBP@PFBT PDs for both 2D and 3D imaging of apoptotic breast cancer cells, thereby offering promising avenues for drug development research.

Despite these advancements, the clinical application of nanoprobes faces several challenges. The production of these nanoprobes on a large scale remains a significant hurdle. Additionally, the metabolic pathways and the fate of these probes post-injection require further elucidation [104]. Furthermore, the inherent limitations of biological autofluorescence interference during imaging and the constraints imposed by classical optical diffraction techniques also pose barriers to their widespread clinical adoption [105].

3.3 Advancements in NIR-II fluorescent probes

The conventional domain of fluorescent probes, which primarily spans the visible light spectrum (400–700 nm) and the NIR-I region (700–900 nm), often faces challenges such as high background interference and limited depth of tissue penetration [106]. In contrast, NIR-II fluorescent probes (1000–1700 nm) offer enhanced tissue penetration, superior resolution, and a more favorable signal-to-background ratio, making them particularly advantageous for

visualizing both physiological and pathological processes in breast cancer [107, 108].

Kang et al. [110] pioneered the synthesis of a novel NIR-II fluorophore, SH1, through a condensation reaction between heptamethine core 9 and the heterocycle indolium salt 6. A standout feature of SH1 is its structure-inherent tumor targeting capability, which differentiates it from traditional dyes that directly target tumor cells. SH1 is first internalized by bone marrow-derived immune cells via fast endophilin-mediated endocytosis, and these immune cells subsequently infiltrate the tumor site (Fig. 6(a)). *In vivo* studies demonstrated that SH1 has a high tumor-to-background ratio of 17.6 in breast cancer mouse models, indicating its potential as an intraoperative imaging agent for breast cancer. In another development, Zhu et al. [111] engineered ErNPs@POL6326, a nano-fluorescent probe that targets CXCR4, a chemokine receptor overexpressed in breast cancer cells and implicated in metastasis. This probe was constructed from erbium ion-doped nanoparticles ($NaErF_4$ core, $NaYF_4$ shell) modified with polyacrylic acid (PAA) and conjugated with balixafortide (POL6326) and demonstrated excellent NIR-II imaging capabilities. The preferential accumulation of ErNPs@6326 in sentinel lymph nodes via CXCR4 binding facilitates the noninvasive identification of metastatic lymph nodes, a crucial aspect in breast cancer management (Fig. 6(b)). This probe is noteworthy for its sensitivity and specificity in detecting sentinel lymph node metastasis in breast cancer models, achieving rates exceeding 92%.

Despite these breakthroughs, NIR-II fluorescent probes still face challenges related to biosafety and biocompatibility, with degradable nanomaterials potentially offering a solution. Additionally, the development of compatible software and hardware systems is essential for clinical applications. The scalability of production and cost considerations also remain significant factors in the clinical translation of these probes [14, 112]. Nevertheless, NIR-II fluorescent probes are potent tools for guiding cancer surgeries and monitoring treatment efficacy.

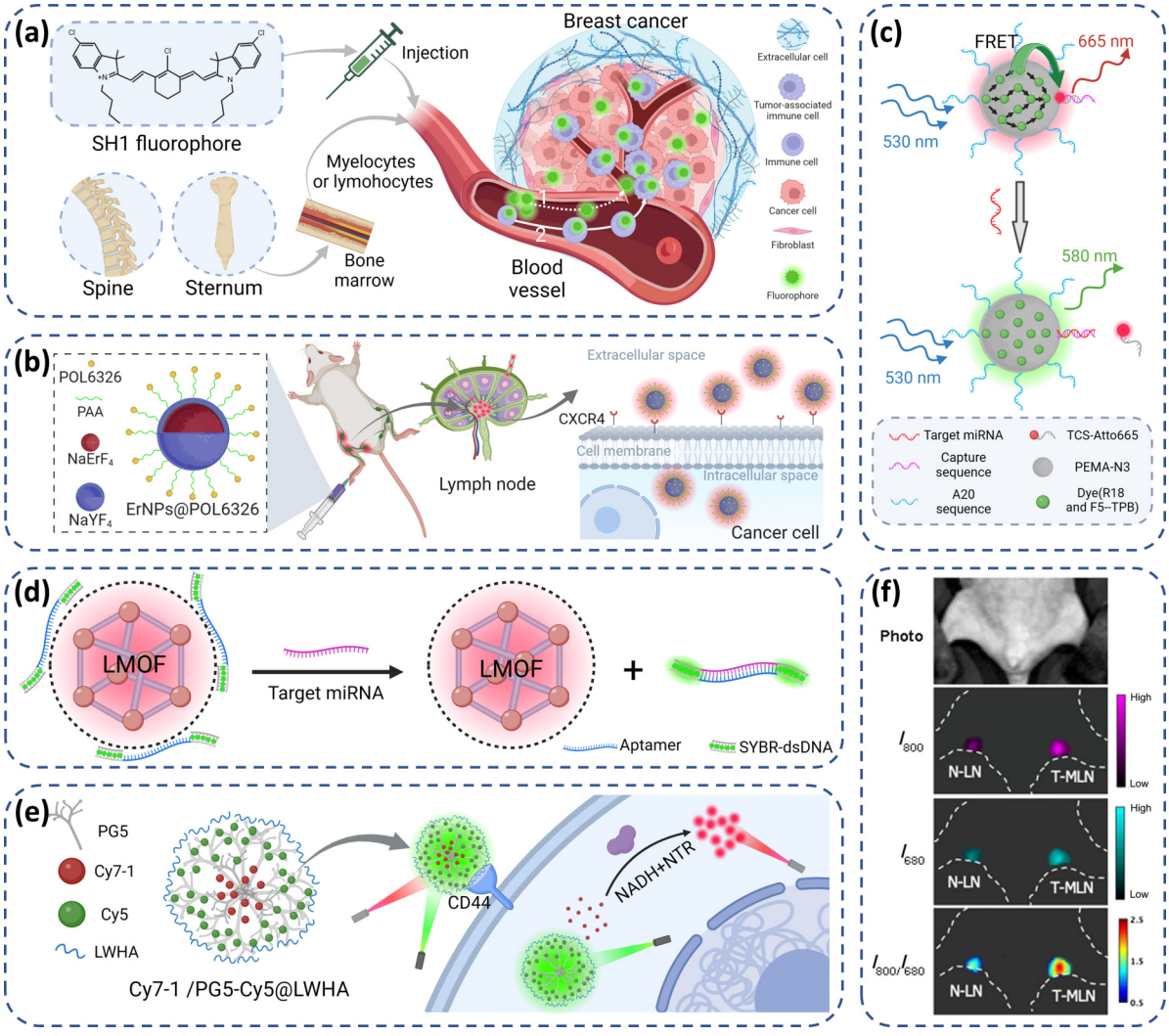

Figure 6 The imaging principles of NIR-II, ratiometric fluorescent probes, and fluorescence images of lymph node metastasis with Cy7-1/PG5-Cy5@LWHA. (a) Schematic of two mechanisms by which SH1 targets tumors: 1) SH1 directly targets cells in the tumor area, 2) SH1 first targets myeloblasts or lymphoblasts and then travels through the blood circulation to reach the tumor area. (b) Flow chart of ErNPs@POL6326 targeting CXCR4 to detect sentinel lymph node metastasis in breast cancer. (c) Schematic of an enzyme-free method based on PEMA-nanoprobe for rapid detection of target miRNAs. (d) Schematic diagram of miRNA detection with probes based on LMOF. (e) Structure and imaging principle of Cy7-1/PG5-Cy5@LWHA. (f) *In vivo* fluorescence images of N-LN and T-MLN at I_{800}, I_{680}, and I_{800}/I_{680}. N-LN is a normal lymph node, and T-MLN is a tumor metastatic lymph node. (f) Reproduced with permission from Ref. [109], © Feng, X. et al. 2022. The figures were created with BioRender.com.

3.4 Innovations in ratiometric fluorescent probes

Ratiometric probes represent a significant advancement in fluorescence imaging, overcoming the limitations of single-emission probes. These limitations, such as instrument variability, probe concentration changes, and environmental influences, can hamper quantitative target molecule detection [45]. Ratiometric probes address these challenges by utilizing the ratio of fluorescence intensities at two distinct emission wavelengths to determine the presence of a target molecule [113]. This method integrates a reference signal and a detection signal within a single entity, enabling self-calibration and producing distinct color changes easily discernible to the human eye [114, 115]. As a result, ratiometric fluorescent probes have become indispensable tools for accurately studying the physiological and pathological functions of target molecules.

3.4.1 miRNA-based ratiometric probes

The detection of miRNAs in cell lysates is a powerful diagnostic tool for breast cancer. Egloff et al. [116] proposed an enzyme-free technique for detecting four miRNAs in T47D, MCF-7, and MCF-10A cell extracts via a poly (ethyl methacrylate) (PEMA)-nanoprobe. These probes were crafted using spherical nanoparticles, whose shell is a poly (ethyl methacrylate)-based polymer azide (PEMA-N3) containing octadecyl rhodamine B (R18) and a bulky hydrophobic counterion F5-TPB. The surface of these nanoparticles was then modified with miRNA capture sequences and 59-fold excess of non-coding A20 sequences, forming a probe that binds with a target-competitive sequence bearing a FRET acceptor (TCS-Atto665). The presence of the target miRNA displaces this sequence, blocking the FRET effect and switching the probe's fluorescence from red to green (Fig. 6(c)). The probes demonstrate high sensitivity and compatibility with portable fluorescence detection devices, whose logarithm of A/(A+D) linearly correlates with the miRNA concentration (A and D are the pick intensities of the acceptor (at 665 nm) and the donor (at 580 nm), respectively).

Wang et al. [42] developed two luminescent metal organic framework (LMOF)-based ratiometric fluorescent probes for detecting elevated levels of miR-21 and miR-155 in breast cancer. One probe, AuNCs@ZIF-8, used gold nanoclusters within a ZIF-8 framework, whereas the other, Zn_2Ph_2Da, utilized Zn^{2+} with organic ligands. Both probes were surface modified with SYBR-dsDNA-labeled miRNA aptamers. In these systems, the fluorescence of surface fluorophores is initially quenched and then recovers upon miRNA binding, while the fluorescence of LMOFs remains constant (Fig. 6(d)).

The ratios of F_{SG}/F_{ZIF} (F_{SG}: fluorescence intensity of SYBR; F_{ZIF}: fluorescence intensity of AuNCs@ZIF-8) and $(F_{522} - F_0)/F_{366}$ (F_{522}: the peak emission intensity of SYBR in the presence of miRNA at 522 nm; F_0: the peak emission intensity of SYBR in the absence of miRNA at 522 nm; F_{366}: the peak emission intensity of Zn_2Ph_2Da at 366 nm) were used as indicators for the detection of miRNA by AuNCs@ZIF-8 and Zn_2Ph_2Da, respectively, showing a good linear relationship with the concentration of the target miRNA. These probes demonstrated high sensitivity and accuracy, as evidenced by their effectiveness in detecting serum miRNA levels in breast cancer mouse models.

These ratiometric probes have increased in precision and utility, highlighting their potential for clinical applications and offering a new dimension in the detection and study of molecular markers in cancer.

3.4.2 Enzymatic ratiometric probes for breast cancer

The relationships between aggressive characteristics—invasion, metastasis, and resistance to treatment—and hypoxia in breast cancer are well established [117]. Within this context, the overexpression of nitroreductase (NTR), which is linked to bioreductive hypoxic conditions in cancer, has emerged as a potential biomarker for breast cancer [118]. Feng et al. [109] innovated an NTR-activated self-calibrating fluorescent probe to quantitatively evaluate hypoxia across different stages of breast cancer, and its effectiveness in detecting metastatic lymph nodes in a mouse breast cancer model was demonstrated. This probe intricately combines a persistently active fluorophore, Cy5, with a poly (amidoamine) dendrimer (5th generation, PG5) to create PG5-Cy5. A second component, Cy7-1, is then encapsulated inside PG5-Cy5, culminating in the formation of the Cy7-1/PG5-Cy5 complex. The exterior of Cy7-1/PG5-Cy5 is subsequently coated with low molecular weight hyaluronic acid (LWHA), resulting in the ratiometric probe Cy7-1/PG5-Cy5@LWHA. In the presence of breast cancer cells, LWHA facilitates the probe's CD44 receptor-mediated endocytosis. The acidic environment within lysosomes triggers structural transformation, resulting in the release of Cy7-1. Under NTR catalysis, Cy7-1 is converted to Cy7 by nicotinamide adenine dinucleotide (NADH), restoring its fluorescence (Fig. 6(e)). The innovation of this probe lies in its ability to provide a fluorescence ratio (I_{800}/I_{680}) of Cy7 to Cy5 that correlates linearly with NTR levels and is unaffected by the probe concentration. This finding was validated in different hypoxic environments and tumor sizes in mice, revealing significant variations in fluorescence ratios. Furthermore, the utility of the probe in detecting lymph node metastasis was confirmed, with a marked increase in the I_{800}/I_{680} ratio within metastatic lymph nodes (Fig. 6(f)).

In a parallel development, Faucher et al. [119] introduced a novel strategy to transform FRET-based activatable fluorescent probes into ratiometric probes. This involves the modification of non-fluorescent receptor groups within the FRET mechanism into fluorophores, leading to the development of two innovative ratiometric probes: 6QC-RATIO, which is responsive to cathepsin, and Death-Cat-RATIO, which is sensitive to both cathepsin and caspase-3 proteases. The operational principle of these probes is based on the FRET effect. In the absence of enzymes, the fluorescence of the donor (Cy5) is quenched, resulting in the fluorescence of only the acceptor (Cy7). Enzymatic activity restores the donor's fluorescence, with the dual-enzyme requirement for Death-Cat-RATIO. Postactivation, the probes accumulate in the lysosomes of tumor-associated macrophages (Fig. 7(a)). The intensity ratio (Cy5/FRET) of Cy5 to Cy7 fluorescence post-enzyme cleavage provides a highly sensitive tumor imaging modality. These probes significantly enhanced imaging in mouse models of subcutaneous breast cancer, offering a highly sensitive and selective imaging approach. Notably, the research team also designed a bespoke imaging system compatible with these probes, comprising a 640 nm laser, a wide-angle diffuser, and multiple cameras. This system was successfully integrated with the FDA-approved da Vinci Xi Surgical System, enabling precise tumor margin visualization and facilitating robotic surgical excision (Fig. 7(b)).

3.4.3 Dual ratiometric Probes for miRNA and enzyme detection

Recent studies have implicated protein tyrosine kinase 7 (PTK7) in the progression and metastasis of breast cancer, primarily through the activation of fibroblast growth factor receptor 1 and epidermal

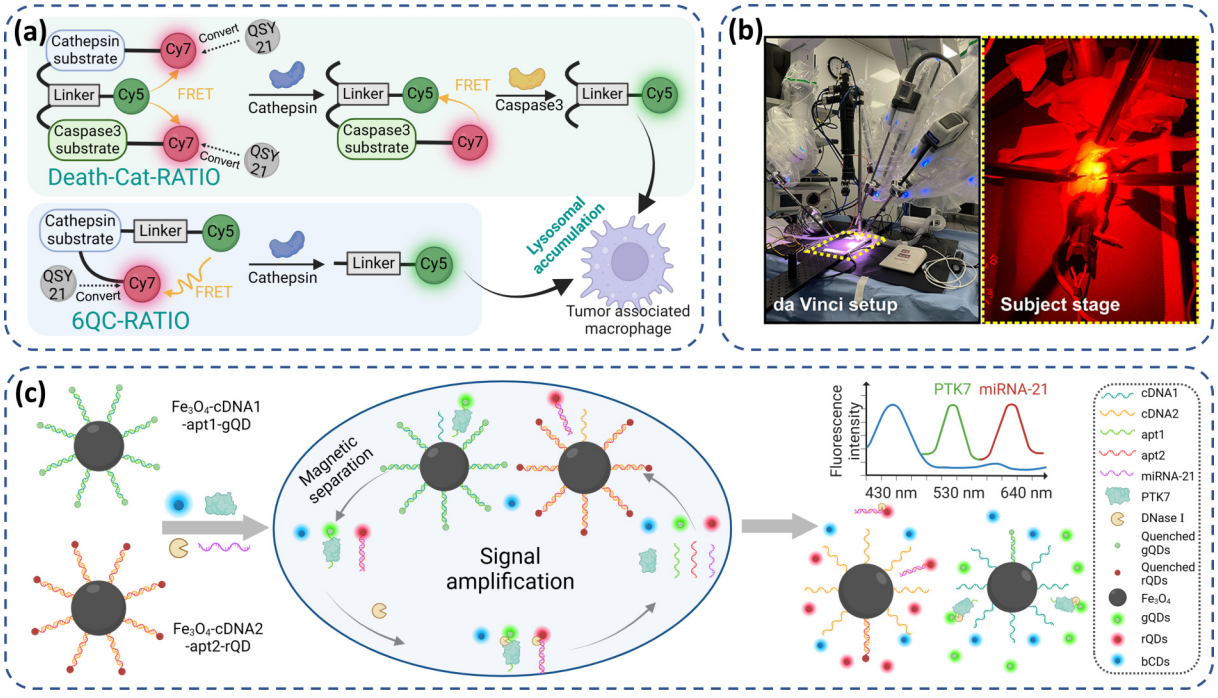

Figure 7 Novel strategies for constructing ratiometric fluorescent probes. (a) Schematic illustration of a strategy for converting a FRET-based activatable fluorescent probe into a ratiometric fluorescent probe and its imaging mechanism. (b) Intraoperative photos of the da Vinci Xi surgical setup with an imaging system based on Death-Cat-RATIO. (c) Flow chart of using a dual-ratio fluorescent probe with a single excitation and triple signals for simultaneously detecting miRNA-21 and PTK7. (b) Reproduced with permission from Ref. [119], © Faucher, F. F. et al. 2023. The figures were created with BioRender.com.

growth factor receptor [120]. In addition, Shi et al. [121] developed a sophisticated dual-ratiometric fluorescent probe capable of simultaneous detection of miRNA and PTK7 via producing triple signals with a single excitation. This probe harnesses amino-modified cDNA sequences coated onto carboxylate-functionalized iron oxide (Fe_3O_4) magnetic nanoparticles. These cDNAs are designed to hybridize with quantum dot-modified aptamers (green QDs (gQDs)-apt1/red QDs (rQDs)-apt2) through complementary base pairing, forming two distinct nanoprobes: Fe_3O_4-cDNA1-apt1-gQD (PTK7 activatable) and Fe_3O_4-cDNA2-apt2-rQD (miR-21 activatable). Initially, the fluorescence of the QDs is suppressed because of the IFE effect. The addition of reference fluorescent boron-doped carbon dots (bCDs) and DNase creates a dynamic sensing platform. In the presence of PTK7 and miR-21, these targets interact with their respective probes, inhibiting the IFE effect and consequently restoring the fluorescence of the gQDs and rQDs. Concurrently, DNase cleaves the unbound aptamers (apt1 and apt2), releasing the targets for a continuous cyclic reaction and thereby amplifying the signal (Fig. 7(c)). The system's effectiveness lies in its ability to measure quantitative changes in fluorescence intensities at specific wavelengths (gQDs at I_{530} and rQDs at I_{640}) against the constant reference fluorescence of bCDs (I_{430}). Therefore, the ratios of I_{530}/I_{430} and I_{640}/I_{430} serve as quantitative indicators for PTK7 and miR-21, respectively. This dual-ratiometric approach demonstrated a robust linear relationship between these ratios and the concentrations of the corresponding target molecules.

The probe's clinical applicability was further confirmed by testing blood samples from patients at various stages of breast cancer (normal, WHO II, and WHO III). This study revealed elevated levels of PTK7 and miR-21 in the WHO II and III groups than in the normal samples. While PTK7 levels did not significantly differ between WHO II and III, miR-21 levels varied considerably across all three groups, suggesting its potential as a stage-specific biomarker for breast cancer. However, the authors noted that further investigation is needed to substantiate this observation.

The ratiometric fluorescent probes compensate for environmental factors and eliminate most ambiguities through an internal reference system, greatly improving accuracy. However, it is difficult to diagnose breast cancer with only one biomarker, and the simultaneous detection of two biomarkers, as described above, is an effective solution. Ratiometric fluorescent probes are also limited by a single imaging mode, so a single probe with different ratio imaging modes will be the way forward [122].

4 Multifunctional fluorescent probes

4.1 Dual-modal imaging probes

Fluorescent probes offer numerous advantages in imaging technologies, yet achieving high sensitivity, deep tissue penetration, and enhanced resolution simultaneously remains a formidable challenge when relying on a single imaging modality [123]. To address this, dual-modal imaging strategies have been adopted, leveraging the complementary strengths of two distinct imaging modalities [124]. This approach significantly enhances imaging capabilities. A notable example is the integration of FL and PA imaging techniques. This combination harnesses the high sensitivity of optical imaging (FL) and the superior tissue penetration depth offered by PA imaging, making it a powerful tool for detailed tissue characterization [125, 126]. Additionally, the synergy between fluorescence imaging and MRI capitalizes on the robust soft tissue contrast of MRI, whereas FL contributes to high temporal and spatial resolution [127]. These dual-modal systems are adept at capturing dual signals from the same molecular target, significantly enhancing the precision and reliability of imaging diagnostics.

4.1.1 *FL/PA-based imaging probes*

In a landmark study, Li et al. [128] introduced a dual-signal FL/PA imaging probe, leveraging the differential expression of urokinase-type plasminogen activator (uPA) in breast cancer cell lines. Elevated uPA levels, which are closely associated with breast cancer progression and metastasis, are present in the invasive MDA-MB-231 cell line but absent in the noninvasive MCF-7 line [129]. This distinction formed the basis for their probe design. Named P-Dex, the probe features a renal clearance enabler, a dual signaling moiety (FL and PA), a self-immolative linker, and a uPA-responsive substrate. Initially, the probe's signal is silenced because of a "caged" hydroxyl group that limits electron donation. Upon encountering uPA, substrate cleavage and subsequent removal of the self-immolative linker restore the electron-donating capability ability of the hydroxyl group, forming CyN_3OH-Dex and triggering concurrent FL and PA signals (Fig. 8(a)).

In vivo trials of P-Dex in mouse models of subcutaneous MDA-MB-231 and MCF-7 breast cancer showed significant NIR fluorescence and PA signals, peaking at 2 h post-injection. A notable decrease in these signals was observed when uPA inhibitors were introduced. Conversely, a control probe (small-molecular probe (SP)), lacking a renal clearance enabler, failed to produce significant signals, highlighting the efficacy of P-Dex (Fig. 8(b)).

Complementing this research, Yin et al. [130] developed the QSY21-GPLGVRGY-Cy5.5 probe. This MMP-2 responsive probe, comprising a cleavable peptide sequence (GPLGVRGY), a near-infrared dye (Cy5.5), and a quencher (QSY21), self-assembles into nanoparticles. Upon MMP-2 interaction, QSY21-GPLGVRGY-Cy5.5 exhibited concentration-dependent fluorescence, providing simultaneous FL and PA imaging capabilities (Fig. 8(c)).

Furthermore, Gao et al. [43] introduced a novel approach to enhancing PA and FL signals through active intramolecular motion (IMM). From TPA-TQ1 to TPA-TQ3, the enhanced IMM increased the thermal-to-acoustic conversion efficiency, thereby enhancing the PA signal, whereas the fluorescence was simultaneously increased via the enhanced AIE effect (Fig. 8(d)). To verify the effectiveness of this approach, TPA-TQ3 was applied to imaging-guided surgery in 4T1 breast tumor-bearing mice. The fluorescent regions labeled by the probe and the bioluminescent regions labeled by luciferase expressed in tumor cells showed excellent consistency, and the results of survival studies also demonstrated the effectiveness of this integrated imaging strategy (Fig. 9(a)). The control group included mice with breast cancer without any surgery, S1 included mice with residual tumor from intraoperative NIR fluorescence imaging, and S2 included mice whose residual tumors were removed until no intraoperative NIR fluorescence signal was detected.

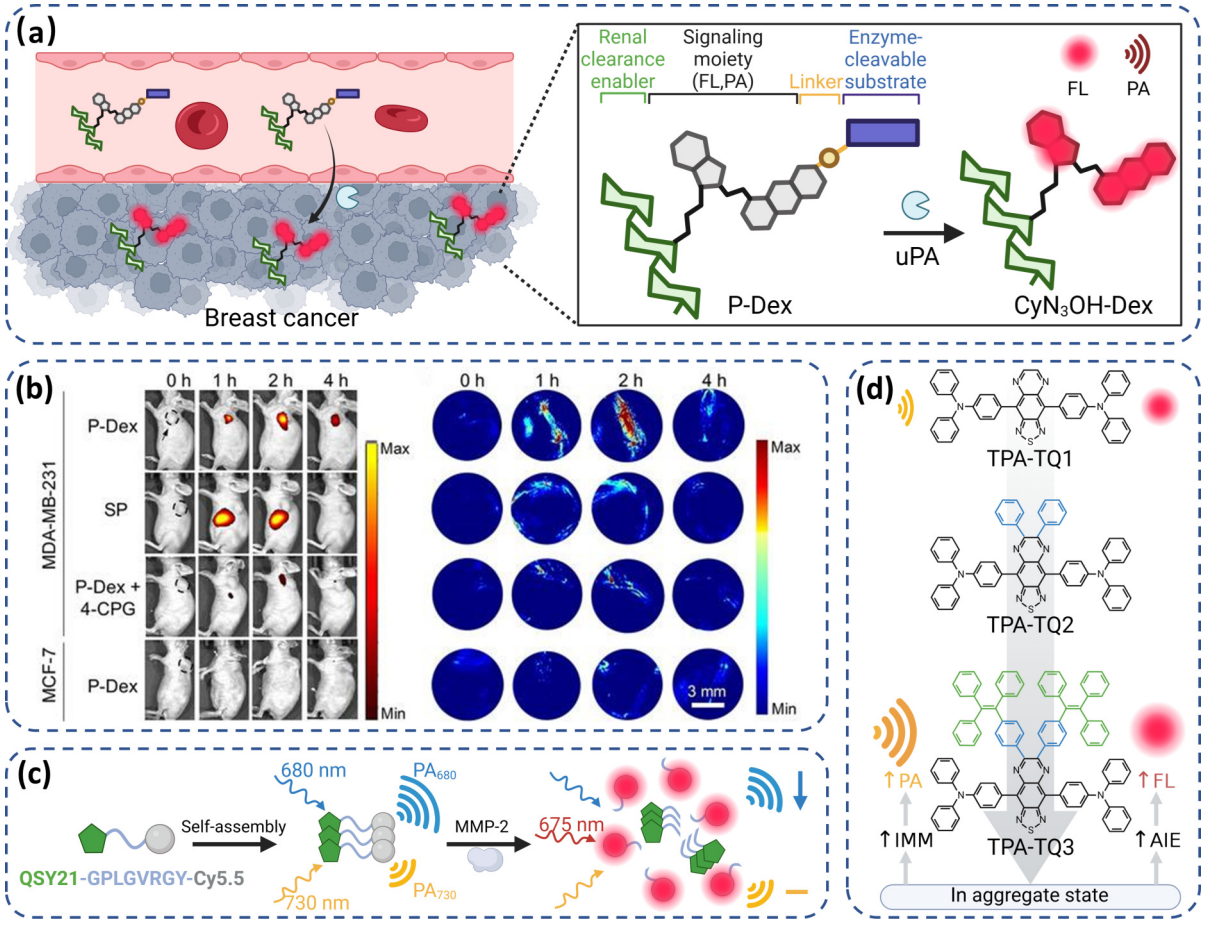

Figure 8 Imaging mechanisms of FL/PA-based fluorescent probes and *in vivo* imaging of a breast tumor with P-Dex. (a) Structure and FL/PA imaging mechanism of P-Dex. (b) Representative NIR fluorescence images (left) and PA images (right) at different time points of MDA-MB-231-tumor-bearing mice treated intravenously with P-Dex, SP, and P-Dex together with the uPA inhibitor 4-CPG, and MCF-7-tumor-bearing mice treated intravenously with P-Dex. (c) Schematic illustration of QSY21-GPLGVRGY-Cy5.5 detecting MMP-2 expression in breast cancer with FL and ratiometric PA signals. (d) A strategy that enhances the PA signal and FL signal of the probe through the active IMM. (b) Reproduced with permission from Ref. [128], © Wiley-VCH Verlag GmbH & Co. KGaA, Weinheim 2020. The figures were created with BioRender.com.

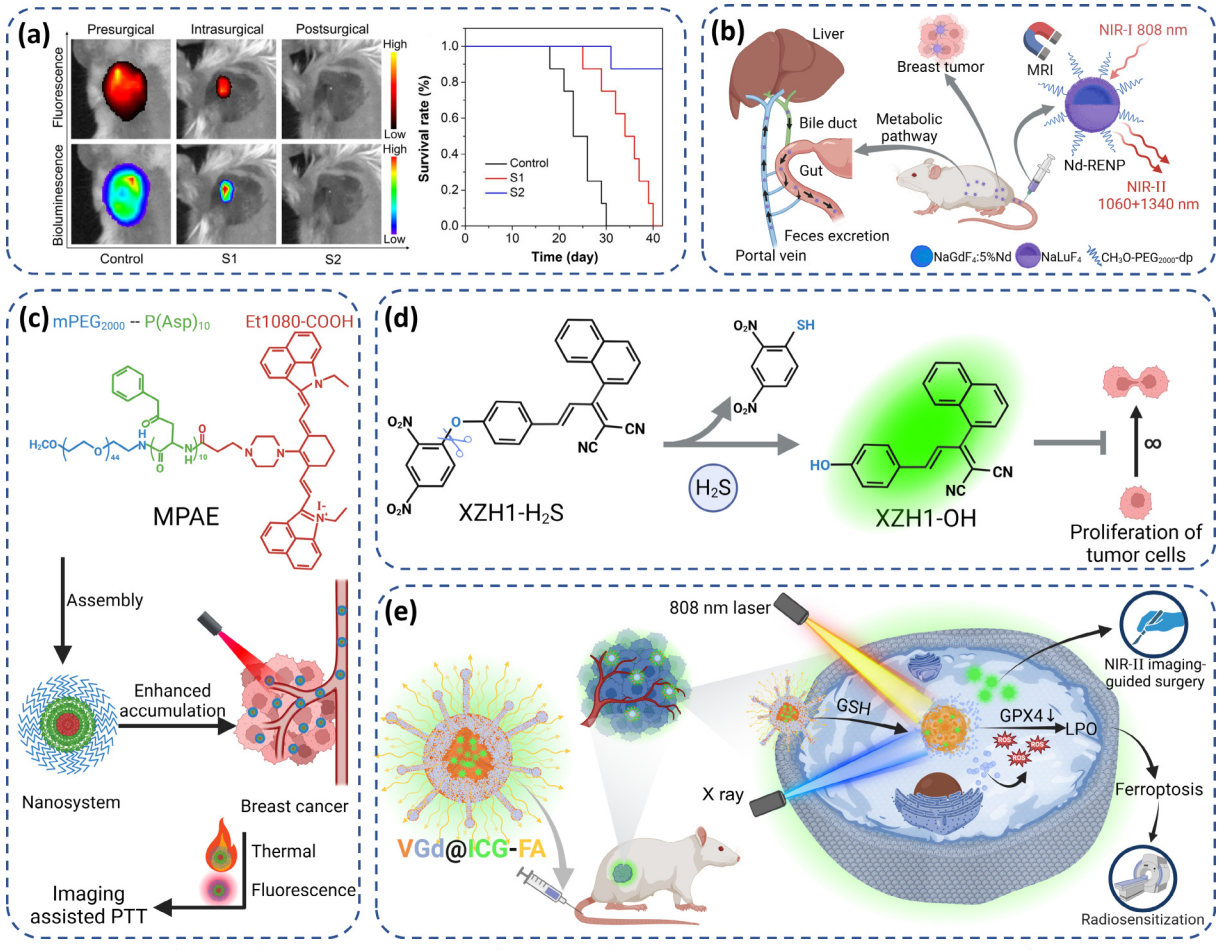

Figure 9 Imaging process of dual-modal (FL/MRI) and theranostic fluorescent probes, along with *in vivo* images and survival curves of imaging-guided tumor surgery with TPA-TQ3. (a) Representative preoperative, intraoperative, and postoperative fluorescence/bioluminescence images (left) and survival curves after different treatments (right) of 4T1 breast tumor-bearing mice (n = 8 mice per group). (b) Diagram of the tumor imaging process and metabolic pathway of Nd-RENPs. (c) Structure of the MPAE and NIR-II fluorescence imaging-assisted PTT strategy. (d) Schematic of XZH1-H_2S recognizing H_2S and inducing apoptosis. (e) Schematic showing the VGd@ICG-FA nanoprobe for NIR-II imaging-guided surgery and enhancing radiotherapy efficacy. (a) Reproduced with permission from Ref. [43], © Wiley-VCH GmbH 2021. The figures were created with BioRender.com.

These pioneering studies exemplify the potential of FL/PA dual-modal imaging probes in breast cancer diagnostics and treatment, offering a nuanced approach to detecting and monitoring tumor progression and facilitating more precise surgical interventions.

4.1.2 FL/MRI dual-modal imaging probes

In the realm of luminescent nanomaterials, rare earth doped nanoparticles stand out because of their chemical stability, facile functional group modification, and transition to near-infrared luminescence, rendering them ideal for biomedical imaging applications [131]. A notable contribution by Wei et al. [132] involved the development of a liver-clearing core–shell nanoprobe for simultaneous fluorescence and magnetic resonance imaging. These Nd^{3+}-doped rare-earth core–shell nanoparticles (Nd-RENPs), featuring a $NaGdF_4$:5%Nd core and $NaLuF_4$ shell, were surface modified with PEG to enhance biocompatibility (Fig. 9(b)). Upon excitation at 808 nm, these probes exhibit two emission peaks in the NIR-II region (1060 and 1340 nm), with the latter offering superior resolution and lower background interference, making them more suitable for tumor imaging.

In summary, it is challenging to provide quantitative or tomographic information and achieve deep penetration depths for fluorescence imaging. Therefore, dual-modal imaging probes have become promising methods for breast cancer diagnosis by overcoming these limitations. For a single probe that integrates dual imaging contrast agents, selecting the right materials, finding a way to assemble the individual components, and achieving excellent properties, which required multiple rounds of optimization, is not easy. Undoubtedly, efforts made will lead to earlier and more accurate diagnosis of breast cancer so that more effective interventions can be implemented [133].

4.2 Theranostic probes

Theranostic probes, which represent a synergistic blend of diagnostic and therapeutic functionalities in a single molecule or nanomaterial, aim to simultaneously detect and treat diseases while minimizing side effects on healthy tissues [134]. Common strategies include the integration of fluorescence imaging with photothermal therapy (PTT), pro-apoptotic drugs, or radiosensitization approaches.

4.2.1 FL/PTT probes

PTT, which leverages heat to eradicate tumor cells, is renowned for its low toxicity and high specificity. Its amalgamation with

fluorescent probes heralds a new era of precision therapy [135, 136]. In this context, Cheng et al. [137] designed a novel NIR-II macromolecular probe, MPAE, tailored for imaging-guided photothermal therapy in breast cancer (Fig. 9(c)). MPAE is synthesized via an amide reaction between the modified dye Et1080-COOH and $mPEG_{2000}$-$P(Asp)_{10}$. The probe exhibited remarkable quenching resistance and formed uniform nanoparticles in an aqueous environment. When administered intravenously, MPAE efficiently accumulates in tumor sites due to its enhanced permeability and retention effect. *In vivo* experiments on breast tumor-bearing mice under 1064 nm irradiation revealed a substantial temperature rise in the tumor region of the MPAE group, significantly outperforming the Et1080-COOH and PBS groups, thereby underscoring its potent imaging-assisted antitumor capability.

4.2.2 FL/Drug-based probes

Chalcone derivatives are known for their diverse biological activities, including anticancer and anti-inflammatory effects, with the added advantage of inducing apoptosis while exerting minimal cytotoxicity [138]. In this context, Xu et al. [139] synthesized a novel hydrogen sulfide (H_2S)-activated organic fluorescent probe. This probe, XZH1-H_2S, initially exhibited quenched fluorescence due to the PET effect. However, in the presence of H_2S, the probe undergoes structural alteration, breaking the ether bond and restoring the hydroxyl group, which reactivates the fluorescence (Fig. 9(d)). Importantly, the chalcone-based fluorescent parent nucleus has antiproliferative effects on MCF-7 cells, resulting in a tumor inhibition rate of 69%. This probe thus concurrently enables imaging and induction of apoptosis in breast cancer cells.

4.2.3 FL/radiosensitization strategy-based probes

Radiotherapy, a cornerstone of breast cancer treatment, functions either by directly damaging DNA with high-energy ionizing radiation or indirectly by generating ROS that induce apoptosis and necrosis [6, 140]. The efficacy of radiotherapy is influenced by several factors, notably the efficient ROS scavenging ability of glutathione (GSH) at high concentrations in cancer cells. Consequently, there has been a surge in developing nanomaterials with radiosensitization strategies that either catalytically produce ROS or consume intracellular GSH [141].

The folic acid (FA) receptor, notably overexpressed in a significant percentage of TNBCs but minimally expressed in normal breast tissue, represents a promising target for cancer therapy [142]. Wei et al. [143] developed a gadolinium-coated silicon dioxide nanoparticle probe, VGd@ indocyanine green (ICG)-FA. This probe contains ICG within the mesoporous of virus-like tetrasulfide bond-doped silica nanoparticles with surface modification of FA. The ability of ICG to target breast cancer cells through FA receptor binding enables these nanoprobes to be utilized for NIR-II imaging-guided surgery. Upon cellular uptake, the high GSH concentrations in the cytoplasm disrupt the tetrasulfide bonds within the nanoparticle framework, leading to GSH depletion, oxidative homeostasis disruption, and enhanced ROS production under X-ray irradiation due to gadolinium. This depletion of GSH also reduces the levels of glutathione peroxidase 4 (GPX4), thus promoting lipid peroxidation accumulation and ferroptosis activation, ultimately enhancing the efficacy of radiotherapy for breast cancer (Fig. 9(e)). The efficacy of NIR-II imaging-guided surgery via VGd@ICG-FA was demonstrated in a residual tumor mouse model. Post-injection, the tumors were initially excised under white light, followed by complete removal of the tissues highlighted by the NIR-II signals. The significantly lower recurrence rate in the VGd@ICG-FA group (12.5%) than in the white light control group (87.5%) and ICG group (75%) underscores the effectiveness of the probe.

Furthermore, angiogenesis, which is critical for tumor growth and metastasis, often involves the overexpression of vascular endothelial growth factor (VEGF) in breast cancer. Bevacizumab, an FDA-approved VEGF-targeting antibody, effectively inhibits angiogenesis and reduces the incidence of metastasis [144, 145]. Zhang et al. [146] synthesized nanoprobes gadolinium-diethylenetriaminepentaacetic acid-human serum albumin@indocyanine green-bevacizumab (NPs-Bev) to increase the efficacy of fluorescence imaging-guided breast-conserving surgery and radiotherapy. The utilization of clinically safe reagents in NPs-Bev endows them with excellent biosafety, making them promising candidates for clinical applications.

The use of theranostic probes offers great potential for reducing the systemic toxicity of drugs and provides a means of visualizing drug delivery, and imaging data can also be used to evaluate therapeutic effects [147]. Some probes are activated by external stimuli, such as photothermal activation, allowing for precise control of the treatment process. Breast cancer-selective theranostic probes are activated in the tumor microenvironment through multiple mechanisms, such as XZH1-H_2S probes [139], which target redox imbalances (H_2S molecules). Currently, most of these strategies have only been preclinical tested, and critical clinical studies are needed to reliably assess their advantages.

5 Applications of fluorescent probes in the treatment of breast cancer

Fluorescent probes have emerged as vital instruments in medical research, particularly in advancing breast cancer treatment strategies. These probes facilitate a comprehensive understanding of breast cancer pathogenesis, drug development, early diagnosis, personalized precision medicine, and fluorescence-guided surgery.

(i) Pathogenesis study. The use of fluorescent probes has significantly enhanced our understanding of breast cancer, propelling advancements in treatment and diagnostic technologies [148]. The probe DCBEM, notable for its robust retention capacity *in vivo*, has successfully delineated breast cancer cell invasion pathways in live mice [68]. Another probe, Cy7-1/PG5-Cy5@LWHA, uses ratio fluorescence signaling to investigate NTR activity, shedding light on the role of hypoxia in breast cancer progression [109]. Additionally, the mitochondrial polar activatable probe PNN is instrumental in exploring breast cancer mechanisms [66].

(ii) Drug development. These probes have streamlined the evaluation of breast cancer treatments. For example, TBP@PFBT PDs have been effective at imaging early apoptosis in breast cancer cells [103]. Guo et al.'s probe construction strategy opens new avenues for targeted drug development [87].

(iii) Early diagnosis. Fluorescent probes offer an efficient, straightforward, and sensitive approach for the early detection of breast cancer. These methods increase the effectiveness of tissue biopsy, which is the gold standard for diagnosis, and provide information on the nature, characteristics, and stage of breast cancer [149]. Probes such as the METTL3/14 detection system [99], nanoflares [80], dual-ratio fluorescent probes [121], probes@MOF-PEG-peps [81], CADA [95], CSUDPs/MoS_2 [84], and PEMA-

nanoprobes [116] have shown promise in early diagnosis, with some being validated in human serum samples.

(iv) Personalized precision medicine. These probes enable real-time monitoring of breast cancer treatment, aiding physicians in customizing patient care while minimizing harm to healthy tissue. The NIR-II probe MPAE, known for its biocompatibility and minimal side effects, has demonstrated exceptional antitumor efficacy in breast tumor-bearing mice [137]. Similarly, ErNPs@POL6326, with its NIR-II imaging capability, has shown high sensitivity and specificity in monitoring sentinel lymph node metastases in a breast cancer model [111]. The theranostic probe XZH1-H_2S simultaneously achieves imaging and apoptosis induction, suggesting new possibilities in breast cancer theranostics [139].

(v) Fluorescence-guided surgery. Fluorescent probes are integral to fluorescence-guided breast cancer surgery, where an external light source is used to excite a fluorescent contrast agent, illuminating the surgical field. These probes aid in delineating tumor margins and detecting residual tumors, thus enhancing surgical precision and outcomes [150]. Probes such as CREKA-GK8-QC [97], TPA-TQ3 [43], VGd@ICG-FA [143], and NPs-Bev [146] have shown exemplary imaging capabilities in mouse models. Additionally, their compatibility with clinical devices, as demonstrated by Faucher et al.'s Death-Cat-RATIO probe and corresponding imaging system, integrated with the FDA-approved da Vinci Xi Surgical System, facilitates robotic excisions, underscoring their potential in facilitating clinical decision-making [119].

6 Conclusions and perspectives

The incidence of breast cancer, which now surpasses that of lung cancer as the most prevalent malignancy among women, continues to rise globally, underscoring the pressing need for advanced imaging and early diagnostic tools. These innovations are crucial for determining breast cancer pathogenesis, enhancing clinical treatment outcomes, and improving patient quality of life. Over the past five years, the rapid development of fluorescent probes, marked by versatile design strategies and unique benefits, has led to significant advances in fluorescence-guided surgery and early breast cancer diagnosis. This timely review encapsulates the latest advancements in this burgeoning field (Table 1).

We delve into the foundational principles, design methodologies, and clinical utilization of diverse fluorescent probes, including molecular, nano, ratiometric, NIR-II, and multifunctional varieties, for breast cancer imaging and diagnosis. The studies featured here aim to steer future probe development toward enhancing breast cancer detection and imaging efficacy. However, the integration of fluorescent probes into clinical practice faces several challenges:

(i) Safety concerns. The *in vivo* metabolic processes and long-term safety of fluorescent probes, particularly when monitoring anticancer efficacy, remain critical areas of focus. Notable examples include the SH1 fluorophore [110] with efficient hepatobiliary

Table 1 Summary of fluorescent probes for breast cancer imaging and early diagnosis

Refs.	Probe	Mode	Mechanism	Biomarker	Fluorophore	$\lambda_{ex}/\lambda_{em}$ (nm)	LOD	Ratio signal	Multifunctional	Application	Other
[66]	PNN	Off-on	ICT	Mitochondria polarity	—[a]	561/582.5 (MCF-10A cell) 561/563.2 (4T1 cell) 561/566.3 (MCF-7 cell)	—	—	—	Imaging in breast cancer mice model (4T1 cells)	Liver clearance
[68]	DCBEM	Off-on	ICT	CYP1A1 (endoplasmic reticulum)	Dicyanoisophorone derivative	419/572 (DCBEM) 550/672 (DCBEM+CYP1A1)	1.66 ng/mL	—	—	Imaging in breast cancer mice model (MCF-7 cells)	—
[80]	Nanoflares	Off-on	—	miR-375 (exosomal miRNA)	Cy5	630/670	0.36 fM	—	—	Detection of serum from breast cancer patients	Using a thermophoretic sensor to amplify fluorescent signals
[81]	Probes@MOF-PEG-peps	Off-on	FRET	miR-21	Fluorescein amidite	488/518	0.54×10^{-9} M	—	—	Detection of MCF-7 cells	Tell 10 mixed MCF-7 cells out of 10^5 MCF-10A cells in serum biomimic samples
				miR-10a	Texas-red	560/614	0.94×10^{-9} M				
[84]	CSUDPs/MoS_2	Off-on	FRET	miR-593	UCNP	980/476	0.17 nM	—	—	Detection of miRNA in Tris-HCl buffer	—
				miR-155		980/540	0.25 nM				
[86]	Anti-HER2-PEG-QDs	Always-on	—	HER2	FeSe QD	365/440 800/440 1080/440	—	—	—	Imaging in breast cancer mice model (MCF-7 cells)	—

(Continued)

Refs.	Probe	Mode	Mechanism	Biomarker	Fluorophore	$\lambda_{ex}/\lambda_{em}$ (nm)	LOD	Ratio signal	Multifunctional	Application	Other
[87]	QD@cMIP	Always-on	—	HER2 GPNMB	QD620 QD520	—/620 —/520	—	—	—	Imaging of MDA-MB-157 cells and MDA-MB-361 cells Imaging in breast cancer mice model (MDA-MB-157 cells)	—
	NIR797 - doped cMIP			GPNMB	NIR797	—					
[95]	CADA	Always-on	—	MUC1	DNA-AgNCs	550/610	3 cells	—	—	Imaging and detection of MCF-7 cells	Dual identification system (fluorescence signal and electrical signal)
[97]	CREKA-GK8-QC	Off-on	—	(MMP-9)-activatable Fibronectin-targeting	Cy5.5	675/690	—	—	—	Imaging-guided surgery in breast cancer mice model (4T1-fLuc cells)	1 mm tumors are detectable
[99]	METTL3/14 detection system	Always-on	—	METTL3/14	Cy5	635/668	2.61×10^{-15} M	—	—	Detection of tissues from breast cancer patients	Based on detection probes and signal probes
[103]	TBP@PFBT PDs	On-off	ACQ	Fe^{3+} Cytochrome C	PDs	460/540	30 pM 32.7 pM	—	—	Imaging in breast cancer mice model (MCF-7 cells)	Take only a few min
[110]	SH1 fluorophore	Always-on	—	—	SH1	808/—	—	—	—	Imaging in breast cancer mice model (E0771 cells)	Tumor-associated immune cells mediated targeting mechanism
[111]	ErNPs@POL6326	Always-on	—	CXCR4 receptor	ErNPs	808/1556	—	—	—	Imaging in breast cancer mice models (4T1-Luc cells and MDA-MB-231-Luc cells)	0.5 mm lymph nodes are detectable
[116]	PEMA-nanoprobes	Ratiometric	FRET	miR-21 miR-222 let-7f miR-30a	R18 Atto665	530/580 (D) 530/665 (A)	4.4 pM 1.7 pM 1.3 pM 1.8 pM	Logarithm of A/(A+D)	—	Detection of cell lysates (T47D cells, MCF-7 cells and MCF-10A cells)	Compatible with portable devices
[42]	AuNCs@ZIF-8 based probes Zn_2Ph_2Da based probes	Ratiometric	FRET	miR-21 miR-21 miR-155	AuNCs@ZIF-8 SYBR Green I Zn_2Ph_2Da SYBR Green I	391/647 (F_{ZIF}) 480/524 (F_{SG}) —/366 (F_{366}) 480/522 (with miRNA: F_{522}; without miRNA: F_0)	0.18 pM 1.85 pM —	F_{SG}/F_{ZIF} $(F_{522}-F_0)/F_{366}$	—	Detection of miRNA in PBS Detection of serum from breast cancer mice models	Take about 10 min
[109]	Cy7-1/PG5-Cy5@LWHA	Ratiometric	—	CD44-targeting NTR-activatable	Cy5 Cy7	640/680 (I_{680}) 745/800 (I_{800})	—	I_{800}/I_{680}	—	Imaging in breast cancer mice model (4T1 cells)	—

(Continued)

Refs.	Probe	Mode	Mechanism	Biomarker	Fluorophore	$\lambda_{ex}/\lambda_{em}$ (nm)	LOD	Ratio signal	Multifunctional	Application	Other
[119]	Death-Cat-RATIO	Ratiometric	FRET	Cathepsin Caspase3	Cy5 Cy7	640/690 (Cy5) 745/790 (FRET)	—	Cy5/FRET	—	Imaging-guided robotic excision in breast cancer mice model (4T1 cells)	—
	6QC-RATIO			Cathepsin						Imaging in breast cancer mice model (4T1 cells)	
[121]	Dual-ratio fluorescent probes	Ratiometric	IFE	miRNA-21 PTK7	gQDs rQDs bCDs	360/530 (I_{530}) 360/640 (I_{640}) 360/430 (I_{430})	0.072 nM 0.426 ng/mL	I_{640}/I_{430} I_{530}/I_{430}	—	Detection of serum from breast cancer patients	—
[128]	P-Dex	Off-on	—	uPA	NIR hemicyanine Dye (CyN_3OH)	695/725	1.5×10^{-5} U/mL	—	FL/PA	Imaging in breast cancer mice model (MDA-MB-231 cells)	Renal clearance
[130]	QSY21-GPLGVRGY-Cy5.5	Off-on	FRET	MMP-2	Cy5.5	675/694	0.52 ng/mL	—	FL/PA	Imaging in breast cancer mice model (4T1 cells)	FL with ratiometric PA signal
[43]	TPA-TQ3	Always-on	—	—	Triphenylamine and Thiadiazoloquinoxa-line	614/820	—	—	FL/PA	Imaging-guided tumor surgery in breast cancer mice model (4T1 cells)	—
[132]	Nd-RENPs	Always-on	—	—	Rare earth (Nd^{3+})-doped nanoparticles	808/1060 808/1340	—	—	FL/MRI	Imaging in breast cancer mice model (4T1 cells)	Liver clearance (within 72 h)
[137]	MPAE	Always-on	—	—	Et1080-COOH	808/1060	—	—	FL/PTT	Imaging-assisted antitumor therapy in breast cancer mice model (4T1 cells)	—
[139]	XZH1-H_2S	Off-on	PET	H_2S	XZH1-OH	488/585	180 nM	—	FL/Drug-Based	Imaging and apoptosis induction in breast cancer mice model (MCF-7 cells)	—
[143]	VGd@ICG-FA	Always-on	—	FA receptor	ICG	808/—	—	—	FL/Radiosensitization Strategy-Based	Imaging-guided surgery in breast cancer mice models (4T1-Luc cells and MMTV-PyMT)	1 mm^3 tumors are detectable
[146]	NPs-Bev	Always-on	—	VEGF-A	ICG	790/796	—	—	FL/Radiosensitization Strategy-Based	Imaging-guided surgery in breast cancer mice models (MDA-MB-231-Luc cells, MMTV-PyVT)	0.5 mm tumors are detectable

[a]Not applicable.

clearance and the P-Dex probe [128], which incorporates a renal-clearance enabler to mitigate toxicity risks.

(ii) Biomarker targeting. Current probes often focus on a single biomarker, yet the multifaceted nature of breast cancer involving multiple biomarkers necessitates probes that can simultaneously target several markers for enhanced accuracy and reduced false positives. An example was given by Shi et al.'s dual-ratio fluorescent probes that concurrently detect PTK7 and miR-21 [121].

(iii) System compatibility. The effective application of fluorescent probes demands complementary hardware and software systems. There is a need for interdisciplinary collaboration to simultaneously develop innovative probes and imaging systems, enhancing clinical applicability. Chen et al.'s integration of Probes@MOF-PEG-peps with droplet microfluidics technology and fluorescent imaging systems exemplify this approach [81].

(iv) Wavelength limitations. To satisfy clinical imaging requirements, the development of probes with NIR-II fluorescence emission capabilities is vital for deeper tissue penetration.

(v) Clinical research. Despite numerous probes in development, only a handful have reached clinical trial stages, with the FDA approving a limited number [151–153]. Future probe design should prioritize clinical needs, considering factors such as cytotoxicity, photostability, and tissue permeability.

(vi) Probe activation. The shift from "always-on" probes to activatable probes is essential to enhance accuracy. Ratiometric probes with self-calibration functions and multimodal probes are promising strategies for addressing the limitations of single-technology approaches and advancing precision medicine.

In conclusion, despite these challenges, the unique benefits of fluorescent probes in breast cancer treatment are undeniable. Continued research in this field is expected to deepen our understanding of breast cancer and herald a new era in cancer therapy.

Data availability

Not applicable.

Acknowledgements

Figures for this article were created with BioRender.com.

Declaration of competing interest

All the contributing authors report no conflict of interests in this work.

Author contribution statement

Q. G.: Conceptualization, writing-original draft. L. T.: Writing-review and editing, visualization. J. Z.: Visualization. Y. Y. X.: Writing-review and editing. F. L.: Conceptualization, supervision, writing-review and editing, and funding acquisition. All the authors have approved the final manuscript.

Informed consent

None.

Ethics statement

None.

Use of AI statement

None.

References

[1] Siegel, R. L.; Miller, K. D.; Fuchs, H. E.; Jemal, A. Cancer statistics, 2022. *CA: Cancer J. Clin.* **2022**, *72*, 7–33.

[2] Nolan, E.; Lindeman, G. J.; Visvader, J. E. Deciphering breast cancer: From biology to the clinic. *Cell* **2023**, *186*, 1708–1728.

[3] Loibl, S.; Poortmans, P.; Morrow, M.; Denkert, C.; Curigliano, G. Breast cancer. *Lancet* **2021**, *397*, 1750–1769.

[4] Giaquinto, A. N.; Sung, H.; Miller, K. D.; Kramer, J. L.; Newman, L. A.; Minihan, A.; Jemal, A.; Siegel, R. L. Breast cancer statistics, 2022. *CA: Cancer J. Clin.* **2022**, *72*, 524–541.

[5] Britt, K. L.; Cuzick, J.; Phillips, K. A. Key steps for effective breast cancer prevention. *Nat. Rev. Cancer* **2020**, *20*, 417–436.

[6] Waks, A. G.; Winer, E. P. Breast cancer treatment. *JAMA* **2019**, *321*, 316.

[7] Yao, N.; Li, W. Q.; Liu, T.; Siyin, S. T.; Chen, X. F.; Wang, W. Q.; Duan, N.; Chen, Y. T.; Qu, J. Primary tumor removal improves the prognosis in patients with stage IV breast cancer: A population-based study (cohort study). *Int. J. Surg.* **2020**, *83*, 109–114.

[8] Pedersen, R. N.; Esen, B. Ö.; Mellemkjær, L.; Christiansen, P.; Ejlertsen, B.; Lash, T. L.; Nørgaard, M.; Cronin-Fenton, D. The incidence of breast cancer recurrence 10–32 years after primary diagnosis. *JNCI: J. Natl. Cancer Inst.* **2022**, *114*, 391–399.

[9] Kuhl, C. K.; Lehman, C.; Bedrosian, I. Imaging in locoregional management of breast cancer. *J. Clin. Oncol.* **2020**, *38*, 2351–2361.

[10] Leon-Ferre, R. A.; Goetz, M. P. Advances in systemic therapies for triple negative breast cancer. *BMJ* **2023**, *381*, e071674.

[11] Li, H. D.; Kim, D.; Yao, Q. C.; Ge, H. Y.; Chung, J.; Fan, J. L.; Wang, J. Y.; Peng, X. J.; Yoon, J. Activity-based NIR enzyme fluorescent probes for the diagnosis of tumors and image-guided surgery. *Angew. Chem., Int. Ed.* **2021**, *60*, 17268–17289.

[12] Mieog, J. S. D.; Achterberg, F. B.; Zlitni, A.; Hutteman, M.; Burggraaf, J.; Swijnenburg, R. J.; Gioux, S.; Vahrmeijer, A. L. Fundamentals and developments in fluorescence-guided cancer surgery. *Nat. Rev. Clin. Oncol.* **2022**, *19*, 9–22.

[13] Choi, H. S.; Kim, H. K. Multispectral image-guided surgery in patients. *Nat. Biomed. Eng.* **2020**, *4*, 245–246.

[14] Yang, R. Q.; Lou, K. L.; Wang, P. Y.; Gao, Y. Y.; Zhang, Y. Q.; Chen, M.; Huang, W. H.; Zhang, G. J. Surgical navigation for malignancies guided by near-infrared-II fluorescence imaging. *Small Methods* **2021**, *5*, 2001066.

[15] Kamal, A. M.; Sakorikar, T.; Pal, U. M.; Pandya, H. J. Engineering approaches for breast cancer diagnosis: A review. *IEEE Rev. Biomed. Eng.* **2023**, *16*, 687–705.

[16] Mann, R. M.; Hooley, R.; Barr, R. G.; Moy, L. Novel approaches to screening for breast cancer. *Radiology* **2020**, *297*, 266–285.

[17] Van Baelen, K.; Geukens, T.; Maetens, M.; Tjan-Heijnen, V.; Lord, C. J.; Linn, S.; Bidard, F. C.; Richard, F.; Yang, W. W.; Steele, R. E. et al. Current and future diagnostic and treatment strategies for patients with invasive lobular breast cancer. *Ann. Oncol.* **2022**, *33*, 769–785.

[18] Li, Y. C.; Chen, Q. H.; Pan, X. Y.; Lu, W.; Zhang, J. New insight into the application of fluorescence platforms in tumor diagnosis: From chemical basis to clinical application. *Med. Res. Rev.* **2023**, *43*, 570–613.

[19] Nasrollahpour, H.; Khalilzadeh, B.; Hasanzadeh, M.; Rahbarghazi, R.; Estrela, P.; Naseri, A.; Tasoglu, S.; Sillanpää, M. Nanotechnology-based electrochemical biosensors for monitoring breast cancer biomarkers. *Med. Res. Rev.* **2023**, *43*, 464–569.

[20] Pradipta, A. R.; Tanei, T.; Morimoto, K.; Shimazu, K.; Noguchi, S.; Tanaka, K. Emerging technologies for real-time intraoperative

margin assessment in future breast-conserving surgery. *Adv. Sci.* **2020**, *7*, 1901519.
[21] Freeman, K.; Geppert, J.; Stinton, C.; Todkill, D.; Johnson, S.; Clarke, A.; Taylor-Phillips, S. Use of artificial intelligence for image analysis in breast cancer screening programmes: Systematic review of test accuracy. *BMJ* **2021**, *374*, n1872.
[22] Crosby, D.; Bhatia, S.; Brindle, K. M.; Coussens, L. M.; Dive, C.; Emberton, M.; Esener, S.; Fitzgerald, R. C.; Gambhir, S. S.; Kuhn, P. et al. Early detection of cancer. *Science* **2022**, *375*, eaay9040.
[23] Li, Y. C.; Chen, Q. H.; Pan, X. Y.; Lu, W.; Zhang, J. Development and challenge of fluorescent probes for bioimaging applications: From visualization to diagnosis. *Top. Curr. Chem.* **2022**, *380*, 22.
[24] Wang, Y. Q.; Hu, Y. X.; Ye, D. J. Activatable multimodal probes for *in vivo* imaging and theranostics. *Angew. Chem., Int. Ed.* **2022**, *61*, e202209512.
[25] Liu, X.; Chang, Y. T. Fluorescent probe strategy for live cell distinction. *Chemical Society Reviews* **2022**, *51*, 1573–1591.
[26] Gao, L. Q.; Wang, W.; Wang, X.; Yang, F.; Xie, L. X.; Shen, J.; Brimble, M. A.; Xiao, Q. C.; Yao, S. Q. Fluorescent probes for bioimaging of potential biomarkers in Parkinson's disease. *Chem. Soc. Rev.* **2021**, *50*, 1219–1250.
[27] Han, H. H.; Tian, H. Jr. ; Zang, Y.; Sedgwick, A. C.; Li, J.; Sessler, J. L.; He, X. P.; James, T. D. Small-molecule fluorescence-based probes for interrogating major organ diseases. *Chem. Soc. Rev.* **2021**, *50*, 9391–9429.
[28] Ding, C. P.; Ren, T. B. Near infrared fluorescent probes for detecting and imaging active small molecules. *Coord. Chem. Rev.* **2023**, *482*, 215080.
[29] Tian, H. Jr. ; Sedgwick, A. C.; Han, H. H.; Sen, S.; Chen, G. R.; Zang, Y.; Sessler, J. L.; James, T. D.; Li, J.; He, X. P. Fluorescent probes for the imaging of lipid droplets in live cells. *Coord. Chem. Rev.* **2021**, *427*, 213577.
[30] Wu, L. L.; Huang, C. S.; Emery, B. P.; Sedgwick, A. C.; Bull, S. D.; He, X. P.; Tian, H.; Yoon, J.; Sessler, J. L.; James, T. D. Förster resonance energy transfer (FRET)-based small-molecule sensors and imaging agents. *Chem. Soc. Rev.* **2020**, *49*, 5110–5139.
[31] Fang, B.; Shen, Y.; Peng, B.; Bai, H.; Wang, L. M.; Zhang, J. X.; Hu, W. B.; Fu, L.; Zhang, W.; Li, L. et al. Small-molecule quenchers for förster resonance energy transfer: Structure, mechanism, and applications. *Angew. Chem., Int. Ed.* **2022**, *61*, e202207188.
[32] Jiang, C. R.; Song, Z. R.; Yu, L. L.; Ye, S. J.; He, H. Fluorescent probes based on macrocyclic hosts: Construction, mechanism and analytical applications. *TrAC Trends Anal. Chem.* **2020**, *133*, 116086.
[33] Chi, W. J.; Chen, J.; Liu, W. J.; Wang, C.; Qi, Q. K.; Qiao, Q. L.; Tan, T. M.; Xiong, K. M.; Liu, X.; Kang, K. et al. A general descriptor ΔE enables the quantitative development of luminescent materials based on photoinduced electron transfer. *J. Am. Chem. Soc.* **2020**, *142*, 6777–6785.
[34] He, H. Y.; Sun, D. W.; Wu, Z. H.; Pu, H. B.; Wei, Q. Y. On-off-on fluorescent nanosensing: Materials, detection strategies and recent food applications. *Trends Food Sci. Technol.* **2022**, *119*, 243–256.
[35] Xiao, Y.; Wu, Z. N.; Yao, Q. F.; Xie, J. P. Luminescent metal nanoclusters: Biosensing strategies and bioimaging applications. *Aggregate* **2021**, *2*, 114–132.
[36] Zhao, X.; Gao, X. M.; Gu, T. Y.; Chen, K. L.; Yan, Z. Y.; Chen, L. J.; Yan, X. P. Recent advances in stimuli-responsive persistent luminescence nanoparticles-based sensors. *TrAC Trends Anal. Chem.* **2023**, *168*, 117279.
[37] Li, X. C.; Zhao, S. J.; Li, B. L.; Yang, K.; Lan, M. H.; Zeng, L. T. Advances and perspectives in carbon dot-based fluorescent probes: Mechanism, and application. *Coord. Chem. Rev.* **2021**, *431*, 213686.
[38] Cai, Y. F.; Ji, X.; Zhang, Y. S.; Liu, C.; Zhang, Z. C.; Lv, Y. J.; Dong, X. C.; He, H. S.; Qi, J. P.; Lu, Y. et al. Near-infrared fluorophores with absolute aggregation-caused quenching and negligible fluorescence re-illumination for *in vivo* bioimaging of nanocarriers. *Aggregate* **2023**, *4*, e277.
[39] Lee, M. M. S.; Yu, E. Y.; Chau, J. H. C.; Lam, J. W. Y.; Kwok, R. T. K.; Wang, D.; Tang, B. Z. Inspiration from nature: BioAIEgens for biomedical and sensing applications. *Biomaterials* **2022**, *288*, 121712.
[40] He, W.; Zhang, Z. C.; Luo, Y. M.; Kwok, R. T. K.; Zhao, Z.; Tang, B. Z. Recent advances of aggregation-induced emission materials for fluorescence image-guided surgery. *Biomaterials* **2022**, *288*, 121709.
[41] Zhang, R. Y.; Huang, X. L.; Chen, C.; Kwok, R. T. K.; Lam, J. W. Y.; Tang, B. Z. AIEgen for cancer discrimination. *Mater. Sci. Eng.: R: Rep.* **2021**, *146*, 100649.
[42] Wang, Y. H.; Shao, Z. S.; Cheng, C.; Wang, J. L.; Song, Z.; Song, W. J.; Zheng, F.; Wang, H. S. Fluorescent oligonucleotide indicators for ratiometric microRNA sensing on metal-organic frameworks. *Chem. Eng. J.* **2022**, *437*, 135296.
[43] Gao, H. Q.; Duan, X. C.; Jiao, D.; Zeng, Y.; Zheng, X. Y.; Zhang, J. T.; Ou, H. L.; Qi, J.; Ding, D. Boosting photoacoustic effect via intramolecular motions amplifying thermal-to-acoustic conversion efficiency for adaptive image-guided cancer surgery. *Angew. Chem., Int. Ed.* **2021**, *60*, 21047–21055.
[44] Duan, Q. J.; Zhao, Z. Y.; Zhang, Y. J.; Fu, L. B.; Yuan, Y. Y.; Du, J. Z.; Wang, J. Activatable fluorescent probes for real-time imaging-guided tumor therapy. *Adv. Drug Deliv. Rev.* **2023**, *196*, 114793.
[45] Park, S. H.; Kwon, N.; Lee, J. H.; Yoon, J.; Shin, I. Synthetic ratiometric fluorescent probes for detection of ions. *Chem. Soc. Rev.* **2020**, *49*, 143–179.
[46] Lei, Z. H.; Zhang, F. Molecular engineering of NIR-II fluorophores for improved biomedical detection. *Angew. Chem., Int. Ed.* **2021**, *60*, 16294–16308.
[47] Yin, X. R.; Cheng, Y. F.; Feng, Y.; Stiles, W. R.; Park, S. H.; Kang, H.; Choi, H. S. Phototheranostics for multifunctional treatment of cancer with fluorescence imaging. *Adv. Drug Delivery Rev.* **2022**, *189*, 114483.
[48] Cheng, H. B.; Li, Y. Y.; Tang, B. Z.; Yoon, J. Assembly strategies of organic-based imaging agents for fluorescence and photoacoustic bioimaging applications. *Chem. Soc. Rev.* **2020**, *49*, 21–31.
[49] Han, X. Y.; Wang, Y.; Huang, Y.; Wang, X. Y.; Choo, J.; Chen, L. X. Fluorescent probes for biomolecule detection under environmental stress. *J. Hazard. Mater.* **2022**, *431*, 128527.
[50] Hu, Z. Y.; Chen, X. Y.; Yang, Y. S.; Wang, S. J.; Hu, Z. G.; Wang, K. Recent advances in the development of fluorescent probes for γ-glutamyltranspeptidase. *Coord. Chem. Rev.* **2024**, *501*, 215562.
[51] Zhang, X. N.; Li, S. S.; Ma, H. Z.; Wang, H.; Zhang, R. P.; Zhang, X. D. Activatable NIR-II organic fluorescent probes for bioimaging. *Theranostics* **2022**, *12*, 3345–3371.
[52] Mei, J.; Tian, H. Most recent advances on enzyme-activatable optical probes for bioimaging. *Aggregate* **2021**, *2*, e32.
[53] Fang, H. B.; Chen, Y. C.; Jiang, Z. Y.; He, W. J.; Guo, Z. J. Fluorescent probes for biological species and microenvironments: From rational design to bioimaging applications. *Acc. Chem. Res.* **2023**, *56*, 258–269.
[54] Nguyen, V. N.; Ha, J.; Cho, M.; Li, H. D.; Swamy, K. M. K.; Yoon, J. Recent developments of BODIPY-based colorimetric and fluorescent probes for the detection of reactive oxygen/nitrogen species and cancer diagnosis. *Coord. Chem. Rev.* **2021**, *439*, 213936.
[55] Welsher, K.; Liu, Z.; Sherlock, S. P.; Robinson, J. T.; Chen, Z.; Daranciang, D.; Dai, H. J. A route to brightly fluorescent carbon nanotubes for near-infrared imaging in mice. *Nat. Nanotechnol.* **2009**, *4*, 773–780.
[56] Li, C. Y.; Chen, G. C.; Zhang, Y. J.; Wu, F.; Wang, Q. B. Advanced fluorescence imaging technology in the near-infrared-II window for biomedical applications. *J. Am. Chem. Soc.* **2020**, *142*, 14789–14804.
[57] Won, M.; Li, M. L.; Kim, H. S.; Liu, P.; Koo, S.; Son, S.; Seo, J. H.;

Kim, J. S. Visible to mid IR: A library of multispectral diagnostic imaging. *Coord. Chem. Rev.* **2021**, *426*, 213608.
[58] Yang, X.; Li, C. C.; Li, P. F.; Fu, Q. R. Ratiometric optical probes for biosensing. *Theranostics* **2023**, *13*, 2632–2656.
[59] Dou, W. T.; Han, H. H.; Sedgwick, A. C.; Zhu, G. B.; Zang, Y.; Yang, X. R.; Yoon, J.; James, T. D.; Li, J.; He, X. P. Fluorescent probes for the detection of disease-associated biomarkers. *Sci. Bull.* **2022**, *67*, 853–878.
[60] Yin, J. L.; Huang, L.; Wu, L. L.; Li, J. F.; James, T. D.; Lin, W. Y. Small molecule based fluorescent chemosensors for imaging the microenvironment within specific cellular regions. *Chem. Soc. Rev.* **2021**, *50*, 12098–12150.
[61] Wang, K.; Liu, C. Y.; Zhu, H. C.; Zhang, Y.; Su, M. J.; Wang, X.; Liu, M. Y.; Rong, X. D.; Zhu, B. C. Recent advances in small-molecule fluorescent probes for diagnosis of cancer cells/tissues. *Coord. Chem. Rev.* **2023**, *477*, 214946.
[62] Liu, C. Y.; Zhu, H. C.; Zhang, Y.; Su, M. J.; Liu, M. Y.; Zhang, X. H.; Wang, X.; Rong, X. D.; Wang, K.; Li, X. W. et al. Recent advances in Golgi-targeted small-molecule fluorescent probes. *Coord. Chem. Rev.* **2022**, *462*, 214504.
[63] Huang, B. H.; Liang, B.; Zhang, R. S.; Xing, D. M. Molecule fluorescent probes for adenosine triphosphate imaging in cancer cells and *in vivo*. *Coord. Chem. Rev.* **2022**, *452*, 214302.
[64] Wang, S.; Ren, W. X.; Hou, J. T.; Won, M.; An, J.; Chen, X. Y.; Shu, J.; Kim, J. S. Fluorescence imaging of pathophysiological microenvironments. *Chem. Soc. Rev.* **2021**, *50*, 8887–8902.
[65] Chen, K.; Lu, P. W.; Beeraka, N. M.; Sukocheva, O. A.; Madhunapantula, S. V.; Liu, J. Q.; Sinelnikov, M. Y.; Nikolenko, V. N.; Bulygin, K. V.; Mikhaleva, L. M. et al. Mitochondrial mutations and mitoepigenetics: Focus on regulation of oxidative stress-induced responses in breast cancers. *Semin. Cancer Biol.* **2022**, *83*, 556–569.
[66] Yin, J. L.; Lin, X. F.; Hu, Q. X.; Huang, S. H. Mitochondrial polarity-triggered fluorogenic optical agent for exploring breast cancer. *Chem. Eng. J.* **2022**, *450*, 138282.
[67] Bouzriba, C.; Chavez Alvarez, A. C.; Gagné-Boulet, M.; Ouellette, V.; Lacroix, J.; Côté, M. F.; C.-Gaudreault, R.; Fortin, S. Branched alkyl of phenyl 4-(2-oxo-3-alkylimidazolidin-1-yl)benzenesulfonates as unique cytochrome P450 1A1-activated antimitotic prodrugs: Biological evaluation and mechanism of bioactivation. *Eur. J. Med. Chem.* **2022**, *229*, 114003.
[68] Liu, T.; Xia, X.; Wang, R.; Rong, X.; Su, Z. H.; Du, J. J.; Fan, J. L.; Peng, X. J.; Sun, W. A fluorescent chemosensor for long-term tracking of cancer cell metastasis and invasion via enzyme-activated anchoring. *Adv. Funct. Mater.* **2023**, *33*, 2304347.
[69] Xu, W.; Zeng, Z. B.; Jiang, J. H.; Chang, Y. T.; Yuan, L. Discerning the chemistry in individual organelles with small-molecule fluorescent probes. *Angew. Chem., Int. Ed.* **2016**, *55*, 13658–13699.
[70] Mirza, Z.; Karim, S. Nanoparticles-based drug delivery and gene therapy for breast cancer: Recent advancements and future challenges. *Semin. Cancer Biol.* **2021**, *69*, 226–237.
[71] Chen, W. Y.; Ni, D. L.; Rosenkrans, Z. T.; Cao, T. Y.; Cai, W. B. Smart H_2S-triggered/therapeutic system (SHTS)-based nanomedicine. *Adv. Sci.* **2019**, *6*, 1901724.
[72] Cheng, M. H. Y.; Mo, Y. L.; Zheng, G. Nano versus molecular: Optical imaging approaches to detect and monitor tumor hypoxia. *Adv. Healthc. Mater.* **2021**, *10*, 2001549.
[73] Zhang, Y.; Li, M. Y.; Gao, X. M.; Chen, Y. H.; Liu, T. Nanotechnology in cancer diagnosis: Progress, challenges and opportunities. *J. Hematol. Oncol.* **2019**, *12*, 1–13.
[74] Ju, J. X.; Xu, D. N.; Mo, X.; Miao, J. Q.; Xu, L.; Ge, G. B.; Zhu, X. Y.; Deng, H. P. Multifunctional polysaccharide nanoprobes for biological imaging. *Carbohydr. Polym.* **2023**, *317*, 121048.
[75] Jouha, J.; Xiong, H. DNAzyme-functionalized nanomaterials: Recent preparation, current applications, and future challenges. *Small* **2021**, *17*, 2105439.
[76] Wang, J. J.; Liu, Y.; Ding, Z.; Zhang, L.; Han, C. Q.; Yan, C. C.; Amador, E.; Yuan, L. Q.; Wu, Y.; Song, C. Y. et al. The exploration of quantum dot-molecular beacon based MoS_2 fluorescence probing for myeloma-related Mirnas detection. *Bioact. Mater.* **2022**, *17*, 360–368.
[77] Sengupta, D.; Deb, M.; Kar, S.; Pradhan, N.; Parbin, S.; Kirtana, R.; Singh, S. P.; Suma, S. G.; Niharika; Roy, A. et al. Dissecting miRNA facilitated physiology and function in human breast cancer for therapeutic intervention. *Semin. Cancer Biol.* **2021**, *72*, 46–64.
[78] Wang, Y. Y.; Yang, Q. Q.; Gao, Z. Q.; Dong, H. F. Recent advance of RNA aptamers and DNAzymes for MicroRNA detection. *Biosens. Bioelectron.* **2022**, *212*, 114423.
[79] Lee, Y.; Ni, J.; Beretov, J.; Wasinger, V. C.; Graham, P.; Li, Y. Recent advances of small extracellular vesicle biomarkers in breast cancer diagnosis and prognosis. *Mol. Cancer* **2023**, *22*, 33.
[80] Zhao, J. X.; Liu, C.; Li, Y. K.; Ma, Y.; Deng, J. Q.; Li, L. L.; Sun, J. S. Thermophoretic detection of exosomal microRNAs by nanoflares. *J. Am. Chem. Soc.* **2020**, *142*, 4996–5001.
[81] Chen, J. Y.; Oudeng, G.; Feng, H. T.; Liu, S. X.; Li, H. W.; Ho, Y. P.; Chen, Y.; Tan, Y.; Yang, M. 2D MOF nanosensor-integrated digital droplet microfluidic flow cytometry for *in situ* detection of multiple miRNAs in single CTC cells. *Small* **2022**, *18*, 2201779.
[82] Zhang, Z.; Zhang, Y. Orthogonal emissive upconversion nanoparticles: Material design and applications. *Small* **2021**, *17*, 2004552.
[83] Zhang, Z.; Chen, Y. M.; Zhang, Y. Self-assembly of upconversion nanoparticles based materials and their emerging applications. *Small* **2022**, *18*, 2103241.
[84] Wu, X.; Li, Y.; Yang, M. Y.; Mao, C. B. Simultaneous ultrasensitive detection of two breast cancer microRNA biomarkers by using a dual nanoparticle/nanosheet fluorescence resonance energy transfer sensor. *Mater. Today Adv.* **2021**, *12*, 100163.
[85] Dhas, N.; Pastagia, M.; Sharma, A.; Khera, A.; Kudarha, R.; Kulkarni, S.; Soman, S.; Mutalik, S.; Barnwal, R. P.; Singh, G. et al. Organic quantum dots: An ultrasmall nanoplatform for cancer theranostics. *J. Controlled Release* **2022**, *348*, 798–824.
[86] Kwon, J.; Jun, S. W.; Choi, S. I.; Mao, X.; Kim, J.; Koh, E. K.; Kim, Y. H.; Kim, S. K.; Hwang, D. Y.; Kim, C. S. et al. FeSe quantum dots for *in vivo* multiphoton biomedical imaging. *Sci. Adv.* **2019**, *5*, eaay0044.
[87] Guo, Z. C.; Xing, R. R.; Zhao, M. H.; Li, Y.; Lu, H. F.; Liu, Z. Controllable engineering and functionalizing of nanoparticles for targeting specific proteins towards biomedical applications. *Adv. Sci.* **2021**, *8*, 2101713.
[88] Yue, D. F.; Wang, M. L.; Deng, F.; Yin, W. T.; Zhao, H. D.; Zhao, X. M.; Xu, Z. C. Biomarker-targeted fluorescent probes for breast cancer imaging. *Chin. Chem. Lett.* **2018**, *29*, 648–656.
[89] Tang, C.; Tong, H. J.; Liu, B.; Wang, X. N.; Jin, Y. S.; Tian, E. L.; Wang, F. Robust ERα-targeted near-infrared fluorescence probe for selective hydrazine imaging in breast cancer. *Anal. Chem.* **2022**, *94*, 14012–14020.
[90] Barman, S.; Ghosh, S.; Roy, R.; Gupta, V.; Ghosh, S.; Ghosh, S. A potent estrogen receptor and microtubule specific purine-benzothiazole-based fluorescent molecular probe induces apoptotic death of breast cancer cells. *Sci. Rep.* **2022**, *12*, 10772.
[91] Zhang, G.; Dong, M.; Yao, X. L.; Xia, Y. K.; Yu, H.; Zhou, Y.; Lian, C.; Zhang, Y. L.; Cui, Y. Y. Advancing breast cancer diagnosis with a near-infrared fluorescence imaging smart sensor for estrogen/progesterone receptor detection. *Sci. Rep.* **2023**, *13*, 21086.
[92] Li, W.; Han, Y. N.; Sun, C. M.; Li, X.; Zheng, J. H.; Che, J. P.; Yao, X. D.; Kufe, D. Novel insights into the roles and therapeutic implications of MUC1 oncoprotein via regulating proteins and non-coding RNAs in cancer. *Theranostics* **2022**, *12*, 999–1011.
[93] Venetis, K.; Invernizzi, M.; Sajjadi, E.; Curigliano, G.; Fusco, N. Cellular immunotherapy in breast cancer: The quest for consistent biomarkers. *Cancer Treatm. Rev.* **2020**, *90*, 102089.

[94] Li, X. Q.; Li, J. W.; Xu, J. R.; Chen, K.; Zhang, Z.; Duan, J. L.; Luo, Q.; Du, Y. F.; Chen, S. Y.; Xie, Y. et al. Nanostructure of functional larotaxel liposomes decorated with guanine-rich quadruplex nucleotide-lipid derivative for treatment of resistant breast cancer. *Small* **2021**, *17*, 2007391.

[95] Cao, Y.; Dai, Y. H.; Chen, H.; Tang, Y. Y.; Chen, X.; Wang, Y.; Zhao, J.; Zhu, X. L. Integration of fluorescence imaging and electrochemical biosensing for both qualitative location and quantitative detection of cancer cells. *Biosens. Bioelectron.* **2019**, *130*, 132–138.

[96] Li, H. N.; Xu, F. X.; Gao, G.; Gao, X.; Wu, B.; Zheng, C.; Wang, P.; Li, Z. L.; Hua, H. M.; Li, D. H. Hydrogen sulfide and its donors: Novel antitumor and antimetastatic therapies for triple-negative breast cancer. *Redox Biol.* **2020**, *34*, 101564.

[97] Cheng, Z. Q.; Jin, Y. S.; Li, J. Q.; Shi, G. Y.; Yu, L. Y.; Shao, B.; Tian, J.; Du, Y.; Yuan, Z. Fibronectin-targeting and metalloproteinase-activatable smart imaging probe for fluorescence imaging and image-guided surgery of breast cancer. *J. Nanobiotechnol.* **2023**, *21*, 112.

[98] Zheng, F. C.; Du, F.; Zhao, J. D.; Wang, X.; Si, Y. R.; Jin, P.; Qian, H. L.; Xu, B. H.; Yuan, P. The emerging role of RNA N6-methyladenosine methylation in breast cancer. *Biomark. Res.* **2021**, *9*, 39.

[99] Zhao, N. N.; Zhang, X. Y.; Zou, X. R.; Zhang, Y.; Zhang, C. Y. Controllable assembly of dendritic DNA nanostructures for ultrasensitive detection of METTL3-METTL14 m^6A methyltransferase activity in cancer cells and human breast tissues. *Biosens. Bioelectron.* **2023**, *228*, 115217.

[100] Liu, M. H.; Zhang, Z.; Yang, Y. C.; Chan, Y. H. Polymethine-based semiconducting polymer dots with narrow-band emission and absorption/emission maxima at NIR-II for bioimaging. *Angew. Chem., Int. Ed.* **2021**, *60*, 983–989.

[101] Bai, X. N.; Wang, K.; Chen, L.; Zhou, J. H.; Wang, J. S. Semiconducting polymer dots as fluorescent probes for *in vitro* biosensing. *J. Mater. Chem. B* **2022**, *10*, 6248–6262.

[102] Szabo, I.; Zoratti, M.; Biasutto, L. Targeting mitochondrial ion channels for cancer therapy. *Redox Biol.* **2021**, *42*, 101846.

[103] Shamsipur, M.; Chabok, A.; Molaabasi, F.; Seyfoori, A.; Hajipour-Verdom, B.; Shojaedin-Givi, B.; Sedghi, M.; Naderi-Manesh, H.; Yeganeh-Faal, A. Label free phosphate functionalized semiconducting polymer dots for detection of iron(III) and cytochrome c with application to apoptosis imaging. *Biosens. Bioelectron.* **2019**, *141*, 111337.

[104] Fitzgerald, R. C.; Antoniou, A. C.; Fruk, L.; Rosenfeld, N. The future of early cancer detection. *Nat. Med.* **2022**, *28*, 666–677.

[105] Li, M. Y.; Zhao, J.; Chu, H. Q.; Mi, Y. S.; Zhou, Z. H.; Di, Z. H.; Zhao, M. P.; Li, L. L. Light-activated nanoprobes for biosensing and imaging. *Adv. Mater.* **2019**, *31*, 1804745.

[106] Zhang, N. N.; Lu, C. Y.; Chen, M. J.; Xu, X. L.; Shu, G. F.; Du, Y. Z.; Ji, J. S. Recent advances in near-infrared II imaging technology for biological detection. *J. Nanobiotechnol.* **2021**, *19*, 132.

[107] Li, B. H.; Zhao, M. Y.; Lin, J.; Huang, P.; Chen, X. Y. Management of fluorescent organic/inorganic nanohybrids for biomedical applications in the NIR-II region. *Chem. Soc. Rev.* **2022**, *51*, 7692–7714.

[108] Wang, Z. A.; Wang, X.; Wan, J. B.; Xu, F. J.; Zhao, N. N.; Chen, M. W. Optical imaging in the second near infrared window for vascular bioimaging. *Small* **2021**, *17*, 2103780.

[109] Feng, X.; Li, Y. H.; Zhang, S. Y.; Li, C. J.; Tian, J. Quantitative hypoxia mapping using a self-calibrated activatable nanoprobe. *J. Nanobiotechnol.* **2022**, *20*, 142.

[110] Kang, H.; Shamim, M.; Yin, X. R.; Adluru, E.; Fukuda, T.; Yokomizo, S.; Chang, H.; Park, S. H.; Cui, Y. N.; Moy, A. J. et al. Tumor-associated immune-cell-mediated tumor-targeting mechanism with NIR-II fluorescence imaging. *Adv. Mater.* **2022**, *34*, 2106500.

[111] Zhu, Y. Y.; Song, L.; Zhang, Y. Q.; Liu, W. L.; Chen, W. L.; Gao, W. L.; Zhang, L. X.; Wang, J. Z.; Ming, Z. H.; Zhang, Y. et al. Development of a rare earth nanoprobe enables *in vivo* real-time detection of sentinel lymph node metastasis of breast cancer using NIR-IIb imaging. *Cancer Res.* **2023**, *83*, 3428–3441.

[112] Meng, X. D.; Pang, X. J.; Zhang, K.; Gong, C. C.; Yang, J. Y.; Dong, H. F.; Zhang, X. J. Recent advances in near-infrared-II fluorescence imaging for deep-tissue molecular analysis and cancer diagnosis. *Small* **2022**, *18*, 2202035.

[113] Sun, J. R.; Cao, X. L.; Lu, W. J.; Wei, Y. C.; Kong, L. X.; Chen, W.; Shao, X. T.; Wang, Y. F. Recent advances in fluorescent probes of peroxynitrite: Structural, strategies and biological applications. *Theranostics* **2023**, *13*, 1716–1744.

[114] Qi, Y. L.; Li, Y. Z.; Tan, M. J.; Yuan, F. F.; Murthy, N.; Duan, Y. T.; Zhu, H. L.; Yang, S. Y. Recent advances in organic near-infrared ratiometric small-molecule fluorescent probes. *Coord. Chem. Rev.* **2023**, *486*, 215130.

[115] Wang, J.; Li, D. Q.; Ye, Y. X.; Qiu, Y.; Liu, J. W.; Huang, L.; Liang, B.; Chen, B. L. A fluorescent metal-organic framework for food real-time visual monitoring. *Adv. Mater.* **2021**, *33*, 2008020.

[116] Egloff, S.; Melnychuk, N.; Reisch, A.; Martin, S.; Klymchenko, A. S. Enzyme-free amplified detection of cellular microRNA by light-harvesting fluorescent nanoparticle probes. *Biosens. Bioelectron.* **2021**, *179*, 113084.

[117] de Heer, E. C.; Jalving, M.; Harris, A. L. HIFs, angiogenesis, and metabolism: Elusive enemies in breast cancer. *J. Clin. Invest.* **2020**, *130*, 5074–5087.

[118] Yu, F. Y.; Shang, X. W.; Zhu, Y.; Lou, H. Y.; Liu, Y. P.; Meng, T. T.; Hong, Y.; Yuan, H.; Hu, F. Q. Self-preparation system using glucose oxidase-inspired nitroreductase amplification for cascade-responsive drug release and multidrug resistance reversion. *Biomaterials* **2021**, *275*, 120927.

[119] Faucher, F. F.; Liu, K. J.; Cosco, E. D.; Widen, J. C.; Sorger, J.; Guerra, M.; Bogyo, M. Protease Activated Probes for Real-Time Ratiometric Imaging of Solid Tumors. *ACS Cent. Sci.* **2023**, *9*, 1059–1069.

[120] Shin, W. S.; Oh, S. W.; Park, H. N.; Kim, J. H.; Lee, S. T. Knockdown of PTK7 reduces the oncogenic potential of breast cancer cells by impeding receptor tyrosine kinase signaling. *Int. J. Mol. Sci.* **2023**, *24*, 12173.

[121] Shi, L. J.; Li, J.; Xiang, Q.; Tan, Y. P.; Zhang, H. Y.; Liu, S. H.; Guo, X. Q.; Zhang, W. J.; Yang, D. Z.; Ma, Y. S. A dual-ratio fluorescent probe with a single excitation triple-signal to synchronously detect PTK7 and miRNA-21 for breast cancer early diagnosis. *Biosens. Bioelectron.* **2023**, *237*, 115529.

[122] Fu, Q. R.; Yang, X.; Wang, M. Z.; Zhu, K.; Wang, Y.; Song, J. B. Activatable probes for ratiometric imaging of endogenous biomarkers *in vivo*. *ACS Nano* **2024**, *18*, 3916–3968.

[123] Fu, Q. R.; Feng, H. J.; Su, L. C.; Zhang, X.; Liu, L. T.; Fu, F. F.; Yang, H. H.; Song, J. B. An activatable hybrid organic-inorganic nanocomposite as early evaluation system of therapy effect. *Angew. Chem., Int. Ed.* **2022**, *61*, e202112237.

[124] Yuan, M.; Wu, Y.; Zhao, C. Y.; Chen, Z. X.; Su, L. C.; Yang, H. H.; Song, J. B. Activated molecular probes for enzyme recognition and detection. *Theranostics* **2022**, *12*, 1459–1485.

[125] Wu, L. Y.; Ishigaki, Y.; Zeng, W. H.; Harimoto, T.; Yin, B. L.; Chen, Y. H.; Liao, S. Y.; Liu, Y. C.; Sun, Y. D.; Zhang, X. B. et al. Generation of hydroxyl radical-activatable ratiometric near-infrared bimodal probes for early monitoring of tumor response to therapy. *Nat. Commun.* **2021**, *12*, 6145.

[126] Jiang, Y. W.; Tang, W. J.; Gao, G.; Geng, Y. Q.; Wu, F. G.; Min, Q. H.; Zhu, J. J. Lipid droplet-hitchhiking probe creates Trojan foam cells for fluorescence/photoacoustic imaging of atherosclerotic plaques. *Biosens. Bioelectron.* **2022**, *216*, 114613.

[127] Chen, B. B.; Liu, M. L.; Huang, C. Z. Recent advances of carbon dots in imaging-guided theranostics. *TrAC Trends Anal. Chem.* **2021**, *134*, 116116.

[128] Li, Q.; Li, S. H.; He, S. S.; Chen, W.; Cheng, P. H.; Zhang, Y.; Miao, Q. Q.; Pu, K. Y. An activatable polymeric reporter for near-infrared fluorescent and photoacoustic imaging of invasive cancer. *Angew. Chem., Int. Ed.* **2020**, *59*, 7018–7023.
[129] Nel, J.; Elkhoury, K.; Velot, É.; Bianchi, A.; Acherar, S.; Francius, G.; Tamayol, A.; Grandemange, S.; Arab-Tehrany, E. Functionalized liposomes for targeted breast cancer drug delivery. *Bioact. Mater.* **2023**, *24*, 401–437.
[130] Yin, L.; Sun, H.; Zhang, H.; He, L.; Qiu, L.; Lin, J. G.; Xia, H. W.; Zhang, Y. Q.; Ji, S. J.; Shi, H. B. et al. Quantitatively visualizing tumor-related protease activity *in vivo* using a ratiometric photoacoustic probe. *J. Am. Chem. Soc.* **2019**, *141*, 3265–3273.
[131] Matulionyte, M.; Skripka, A.; Ramos-Guerra, A.; Benayas, A.; Vetrone, F. The coming of age of neodymium: Redefining its role in rare earth doped nanoparticles. *Chem. Rev.* **2023**, *123*, 515–554.
[132] Wei, Z. X.; Duan, G. X.; Huang, B. X.; Qiu, S. S.; Zhou, D. D.; Zeng, J. F.; Cui, J. B.; Hu, C. H.; Wang, X. M.; Wen, L. et al. Rapidly liver-clearable rare-earth core-shell nanoprobe for dual-modal breast cancer imaging in the second near-infrared window. *J. Nanobiotechnol.* **2021**, *19*, 369.
[133] Zhao, J. H.; Chen, J. W.; Ma, S. N.; Liu, Q. Q.; Huang, L. X.; Chen, X. N.; Lou, K. Y.; Wang, W. Recent developments in multimodality fluorescence imaging probes. *Acta Pharm. Sin. B* **2018**, *8*, 320–338.
[134] Mao, D.; Liu, B. Biology-oriented design strategies of AIE theranostic probes. *Matter* **2021**, *4*, 350–376.
[135] Dai, Y.; Mei, J. W.; Li, Z.; Kong, L. T.; Zhu, W. B.; Li, Q. M.; Wu, K. R.; Huang, Y.; Shang, X. F.; Zhu, C. Acidity-activatable nanoparticles with glucose oxidase-enhanced photoacoustic imaging and photothermal effect, and macrophage-related immunomodulation for synergistic treatment of biofilm infection. *Small* **2022**, *18*, 2204377.
[136] Yan, C. X.; Zhang, Y. T.; Guo, Z. Q. Recent progress on molecularly near-infrared fluorescent probes for chemotherapy and phototherapy. *Coord. Chem. Rev.* **2021**, *427*, 213556.
[137] Cheng, Q.; Tian, Y. L.; Dang, H. P.; Teng, C. C.; Xie, K.; Yin, D. L.; Yan, L. F. Antiquenching macromolecular NIR-II probes with high-contrast brightness for imaging-guided photothermal therapy under 1064 nm irradiation. *Adv. Healthc. Mater.* **2022**, *11*, 2101697.
[138] Yin, F. X.; Zhao, R.; Gorja, D. R.; Fu, X. R.; Lu, N.; Huang, H.; Xu, B. B.; Chen, H. Y.; Shim, J. H.; Liu, K. D. et al. Novel dual inhibitor for targeting PIM1 and FGFR1 kinases inhibits colorectal cancer growth *in vitro* and patient-derived xenografts *in vivo*. *Acta Pharm. Sin. B* **2022**, *12*, 4122–4137.
[139] Xu, Z.; Zheng, Y.; Qiao, R. R.; Cao, S. R.; Fang, Y.; Bo, X. M.; Zhu, H. L.; Ying, C. J.; Sun, Y.; Zheng, J. N. Organic fluorescent probe for concurrent imaging and apoptosis induction in cancer cells *in vivo* and *in vitro* by utilizing endogenous hydrogen sulfide. *Chem. Eng. J.* **2023**, *456*, 141000.
[140] Petroni, G.; Cantley, L. C.; Santambrogio, L.; Formenti, S. C.; Galluzzi, L. Radiotherapy as a tool to elicit clinically actionable signalling pathways in cancer. *Nat. Rev. Clin. Oncol.* **2022**, *19*, 114–131.
[141] Xie, J. N.; Gong, L. J.; Zhu, S.; Yong, Y.; Gu, Z. J.; Zhao, Y. L. Emerging strategies of nanomaterial-mediated tumor radiosensitization. *Adv. Mater.* **2019**, *31*, 1802244.
[142] Scaranti, M.; Cojocaru, E.; Banerjee, S.; Banerji, U. Exploiting the folate receptor α in oncology. *Nat. Rev. Clin. Oncol.* **2020**, *17*, 349–359.
[143] Wei, M.; Bai, J. W.; Shen, X.; Lou, K. L.; Gao, Y. Y.; Lv, R. C.; Wang, P. Y.; Liu, X. L.; Zhang, G. J. Glutathione-exhausting nanoprobes for NIR-II fluorescence imaging-guided surgery and boosting radiation therapy efficacy via ferroptosis in breast cancer. *ACS Nano* **2023**, *17*, 11345–11361.
[144] Zhu, Y. X.; Hu, Y. X.; Tang, C. J.; Guan, X. X.; Zhang, W. W. Platinum-based systematic therapy in triple-negative breast cancer. *Biochim. Biophys. Acta (BBA) - Rev. Cancer* **2022**, *1877*, 188678.
[145] Shashni, B.; Nishikawa, Y.; Nagasaki, Y. Management of tumor growth and angiogenesis in triple-negative breast cancer by using redox nanoparticles. *Biomaterials* **2021**, *269*, 120645.
[146] Zhang, Y. Q.; Liu, W. L.; Luo, X. J.; Shi, J. P.; Zeng, Y. Z.; Chen, W. L.; Huang, W. H.; Zhu, Y. Y.; Gao, W. L.; Li, R. H. et al. Novel self-assembled multifunctional nanoprobes for second-near-infrared-fluorescence-image-guided breast cancer surgery and enhanced radiotherapy efficacy. *Adv. Sci.* **2023**, *10*, 2205294.
[147] Sharma, A.; Verwilst, P.; Li, M. L.; Ma, D. D.; Singh, N.; Yoo, J.; Kim, Y.; Yang, Y.; Zhu, J. H.; Huang, H. Q. et al. Theranostic fluorescent probes. *Chem. Rev.* **2024**, *124*, 2699–2804.
[148] Liu, H. W.; Chen, L. L.; Xu, C. Y.; Li, Z.; Zhang, H. Y.; Zhang, X. B.; Tan, W. H. Recent progresses in small-molecule enzymatic fluorescent probes for cancer imaging. *Chem. Soc. Rev.* **2018**, *47*, 7140–7180.
[149] Zhang, Y.; Zhang, G. P.; Zeng, Z. L.; Pu, K. Y. Activatable molecular probes for fluorescence-guided surgery, endoscopy and tissue biopsy. *Chem. Soc. Rev.* **2022**, *51*, 566–593.
[150] Liu, R. F.; Xu, Y. X.; Xu, K.; Dai, Z. F. Current trends and key considerations in the clinical translation of targeted fluorescent probes for intraoperative navigation. *Aggregate* **2021**, *2*, e23.
[151] Refaat, A.; Yap, M. L.; Pietersz, G.; Walsh, A. P. G.; Zeller, J.; del Rosal, B.; Wang, X. W.; Peter, K. *In vivo* fluorescence imaging: Success in preclinical imaging paves the way for clinical applications. *J. Nanobiotechnol.* **2022**, *20*, 450.
[152] Seah, D.; Cheng, Z. M.; Vendrell, M. Fluorescent probes for imaging in humans: Where are we now. *ACS Nano* **2023**, *17*, 19478–19490.
[153] Hernot, S.; van Manen, L.; Debie, P.; Mieog, J. S. D.; Vahrmeijer, A. L. Latest developments in molecular tracers for fluorescence image-guided cancer surgery. *Lancet Oncol* **2019**, *20*, e354–e367.